HHS Public Access

Author manuscript

Adv Healthc Mater. Author manuscript; available in PMC 2021 May 01.

Published in final edited form as:

Adv Healthc Mater. 2020 May ; 9(9): e1901058. doi:10.1002/adhm.201901058.

Magnetic nanoparticles in cancer therapy and diagnosis

Dr. A. Farzin,
Division of Engineering in Medicine, Department of Medicine, Brigham and Women's Hospital, Harvard Medical School, Boston, MA 02139, USA

Mr. S. Alireza Etesami,
Department of Mechanical Engineering, The University of Memphis. Memphis, TN 38152, USA

Mr. Jacob Quint,
Department of Mechanical and Materials Engineering, University of Nebraska, Lincoln, Lincoln, NE, 68588, USA

Dr. Adnan Memic,
Department of Biomedical Engineering, University of Connecticut, Farmington, CT, 06030, USA

Prof. Ali Tamayol*
Division of Engineering in Medicine Department of Medicine, Brigham and Women's Hospital, Harvard Medical School, Boston, MA 02139, USA

Department of Mechanical and Materials Engineering, University of Nebraska, Lincoln, Lincoln, NE, 68588, USA

Department of Biomedical Engineering, University of Connecticut, Farmington, CT, 06030, USA

Abstract

There is urgency for the development of nanomaterials that can meet emerging biomedical needs. Magnetic nanoparticles (MNPs) offer high magnetic moments and surface-area-to-volume ratios that make them attractive for hyperthermia therapy of cancer and targeted drug delivery. Additionally, they can function as contrast agents for magnetic resonance imaging (MRI) and can improve the sensitivity of biosensors and diagnostic tools. Recent advancements in nanotechnology have resulted in the realization of the next generation of MNPs suitable for these and other biomedical applications. This review discusses methods utilized for the fabrication and engineering of MNPs. Recent progress in the use of MNPs for hyperthermia therapy, controlling drug release, MRI, and biosensing is also critically reviewed. Finally, challenges in the field, potential opportunities for the use of MNPs towards improving their properties are discussed.

Keywords

Magnetic nanoparticles; cancer therapy; hyperthermia; drug delivery; cancer detection

*Corresponding author: A. Tamayol, atamayol@uchc.edu (A. Tamayol).

1. Introduction

Micro and nanoparticles (NPs) made from lipids, polymers, and metals have been used in biomedical applications for decades [1]. In recent years, various studies have demonstrated the importance of the size of NPs on their function *in vivo*. Recent advancements have enabled the fabrication of NPs with low polydispersity and size as small as 10 nm in diameter [2]. NPs of 10–100 nm have gained significant attention in biomedical engineering due to their physical and chemical properties [3]. These NPs offer extremely high surface-area-to-volume ratios. NPs larger than 100 nm can be consumed by immune cells; therefore, large NPs have reduced availability in blood flow and tissues [4], whereas particles smaller than 10 nm can easily be filtered out through the kidneys [5]. However, NPs in the size range of 10–100 nm offer suitable residence time in the blood which grants high potential for systemic therapies [6].

Magnetic nanoparticles (MNPs) are an important class of NPs that are typically fabricated from pure metals (Fe, Co, Ni, and some rare earth metals) or a mixture of metals and polymers [7]. The utilization of MNPs has increased in many medical applications, namely hyperthermia cancer treatment [8], controlled drug release [9], magnetic resonance imaging (MRI) [10], and biosensing [11]. A key advantage of MNPs is their capacity to be magnetically manipulated from an external magnetic field. Chemical composition, size, shape, morphology, and magnetic behavior of the MNPs are the most important criteria in determining their biomedical applications [12]. Additionally, magnetic properties and MNP effectiveness *in vivo* can be tailored by applying a safe and biocompatible coating to increase their acceptability for a specific target in the human body [13]. This coating provides surface chemistry that aids in the integration of functional ligands [14]. Modifying the surface chemistry can result in the multifunctionality of MNPs. For instance, chemical modification provides multiplexed functionality such as combined hyperthermia-drug delivery [15] and multimodal imaging [14].

In the 19th century, it was found that fever can negatively impact the growth of cancer cells [16]. It was shown that cancerous and non-cancerous cells display different behavior over a temperature range of 42–45°C (i.e. hyperthermia). Healthy cells can withstand these temperatures for a short period of time while cancerous cells undergo apoptosis [17]. Therefore, maintaining the temperature of the cellular environment in hyperthermia could represent an effective method in treating cancer with fewer adverse effects [18]. MNPs hold great potential for generating heat under an applied magnetic field and elevating the temperature of the cancerous tumor to 42–45°C. Currently, hyperthermia is employed in treating numerous cancers, namely prostate, uterine, lung, and neck cancers [19].

A key concern of current cancer chemotherapies is their inability, once systematically administered, to distinguish between cancerous and healthy cells that often results in the death of both cell types. Therefore, numerous research efforts have been dedicated to identifying strategies to deliver drugs to only cancerous cells while maintaining the viability of surrounding healthy cells [20]. MNPs have been identified as a potential solution to this major challenge as they can modify the pharmacokinetics of drugs to decrease cytotoxicity and increase the releasing time and half-life of drugs [21]. In addition to the possibility of

localizing MNPs at the cancerous area by a magnetic field [22], they can be decorated with high-affinity ligands (i.e. biological molecules such as peptides and antibodies that have an ability for detecting cancerous cells) to further improve their selectivity [23].

Another application of MNPs is in MRI to improve the image contrast of targeted tissues. MNPs can be localized into the tissue site to increase proton relaxation and to enhance their visibility [24]. Considered as a next-generation material in MRI, MNPs used for imaging consist of nanocrystalline particles that can be further functionalized with biocompatible coatings and ligands.

More efficient and precise measurement of biomarkers and cells is vital in rapid disease diagnosis and cancer metastasis prevention. Cancer diagnosis in early stages can significantly prevent cancer tumor growth and its metastasis to other tissues [25]. Cancer evaluation tools with high sensitivity in the detection of several diverse targeting moieties that require minimal sample preparation contribute significantly to rapid diagnosis. Recently, the application of the MNPs in biosensors has been extensively studied. These systems offer unique advantages over traditional detection methods [26].

Although there are several review papers discussing the use of MNPs for cancer treatment [27], strategies for pairing diagnosis and treatment have not been properly reviewed. In this review, various methods for the fabrication of MNPs are briefly discussed, and the advantages and shortcomings of MNPs are listed. Various utilization of MNPs in cancer treatment through hyperthermia and targeted drug delivery and release are reviewed. Here, we consider recent advancements in combined cancer treatments like hyperthermia and drug release by the MNPs. We have shown that MNPs in different forms of micelles, liposomes, and core/shell structures have demonstrated a significant capability in hyperthermia, drug delivery, and MRI applications [28] (Figure 1). Additionally, the discussion of the potential of MNPs in cancer diagnosis by magnetic resonance imaging and biosensors is provided. Finally, the limitations of these therapies and potential areas that MNPs in their existing form or improved versions can impact cancer treatment or diagnosis will be highlighted.

2. Methods for the fabrication of MNPs

One of the essential requirements when developing new materials at the intersection of several fields like nanotechnology, biomaterials, and engineering is the ability to control and tailor the properties of the system to the specific application. Reproducibility and predictability of the synthesis and fabrication processes are equally important for their clinical application. The production of MNPs with desirable morphology, particle size, shape, and distribution has been extensively investigated [29]. Among many approaches, MNPs are primarily fabricated using co-precipitation [30], microemulsion [31], and high temperature based [32] methods.

One of the most frequently used methods, especially when trying to achieve spherical MNPs, is co-precipitation from aqueous solution [33]. By this method, various oxidizing agents oxidize ferrous hydroxide suspensions. It is reported that by using this method, spherical MNPs can be achieved in the range of 30–100 nm [34]. Furthermore, these two

primary factors can significantly affect the chemical composition and electrostatic surface charge of the formed particles. For example, NPs obtained by this method, due to large surface-area-to-volume ratios, often strongly aggregate. Stabilizing NPs by coating their surface with surfactants such as proteins [35], nonionic detergents, or polyelectrolytes [36] can prevent their aggregation. An alternative strategy to co-precipitation is based on water in oil microemulsion systems where fine micro-droplet dispersions of one liquid with surfactant molecules are placed in another immiscible liquid.

MNPs typically cannot carry compounds, so various composite systems made of polymers or gels and MNPs have been synthesized to allow for easy manipulation *in vivo* and to carry hydrophilic or hydrophobic compounds. The surfaces of MNPs can also be functionalized with molecules such as amine and thiol groups that facilitate the binding of drugs or targeting ligands for targeting specific tissues and cell types. Table 1 provides an overall picture of current types of MNP-based composite systems and their applications in cancer diagnosis and treatment.

3. Cancer therapy

3.1. Hyperthermia

The induction of MNPs by exposure to an appropriate alternating magnetic field (AMF) is being investigated in the application of targeted therapeutic heating of cancer cells [27a, 47]. Hyperthermia is a therapeutic technique where the temperature in a specific tissue or the entire body is raised above normal physiological temperatures. The heat generated from MNPs causes cells in a tumor to die [48]. Cancerous cells are sensitized to hyperthermia compared to normal cells, due to the lowering of the pH at the cancerous microenvironment, which results in decreased thermotolerance [49]. A disorganized vascular network and lower blood flow within the cancerous tissue lowers the rate of convective cooling of the tumor and cause the tumor to overheat. On the other hand, healthy tissue possessing organized blood flow can dissipate extra heat to neighboring tissue through conduction and convection [50]. As a result, the viability of cells in the cancerous tissue significantly decreases between 41°C-46 °C, whereas healthy tissues are able to successfully dissipate the heat and the cells there can survive [51]. The generation of heat in standard hyperthermia treatment can be from ultrasonic waves, radiofrequency, microwaves, infrared radiation, and hot water [52]. Although the hyperthermia techniques present a considerable advancement in clinical procedures, they have several side effects including blisters, burns, pain, and unregulated tissue growth [52b]. Alternatively, localized hyperthermia by MNPs is shown to have fewer adverse effects. Researchers have investigated the effectiveness of this approach in animal studies and have devised strategies to locally increase the temperature of tissue as a means of cancer treatment [53]. Inducing MNP based hyperthermia is also being investigated as an adjuvant to conventional cancer therapeutic methods such as chemotherapy and radiation therapy [54].

Hyperthermia therapy is used to increase temperature locally or systemically based on the extent of the area under treatment. Ideally, local hyperthermia is used to only increase the temperature of unhealthy tissue such as cancerous tumors. Most local hyperthermia methods without the use of MNPs are not considered effective in treating cancer tumors because they

fail to produce a homogenous distribution of temperature within and cause avert overheating of deeply embedded parts of cancerous tissue [55]. Accordingly, advances in nanotechnology have led to improved safety, feasibility, and effectiveness of local hyperthermia therapy for treating cancerous tissues [56]. MNPs with high levels of magnetism have displayed excellent behavior in producing heat at regions of cancerous tissue [57]. These MNPs can be either inserted directly into the cancerous tissue by injection or localized at the area of tumor from manipulation via a magnetic field. Then, the particles are heated by applying an AMF. Concentrated heat at the cancerous site is generated by the directed MNPs in hyperthermia treatment (magnetic hyperthermia), cancerous cell death occurs and can be considered as an efficient method in treating tumors.

Recently, *in vivo* experiments to study the influence of magnetic hyperthermia on the size of cancerous tumors have gained considerable attention in cancer treatment. Basel *et al.* [58] generated pancreatic cancer tissue in mice via injection of murine pancreatic carcinoma cell line Pan02 cells. After several days of tumor growth, monocyte/macrophage-like cells loaded with IONPs were injected into the mice. After three days, the MNPs present in cancerous tissue produced heat under an AMF stimulation. They reported a significant reduction in tumor volume over time. Similarly, Araya *et al.* [59] synthesized superparamagnetic IONPs coated with carboxydextran for hyperthermia applications. A549 cells (i.e. non-small cell lung cancer cell line) were injected in BALB/c nu/nu athymic mice along with exposure to AMF for 20 min (temperature inside cancer tissue was recorded 43–45 ºC). It was observed that tumor volume was notably decreased. Most of these studies have shown positive effects of hyperthermia treatment in reducing cancer tissue volume when MNPs are directly or intravenously injected in the tumor followed by AMF exposition [60]. Thorat *et al.* developed highly dispersible $La_{0.7}Sr_{0.3}MnO_3$ magnetic nanoparticles with high self-heating capacity under external AMF [61]. Magnetic hyperthermia has shown high efficiency in suspending cancer cell growth. Kolosnjaj *et al.* [62] showed the ability to impede cancer growth by using MNPs in epidermoid carcinoma mice. They reported that chemotherapy can be more effective by using MNPs. This way, drug penetration into cancer cells is improved through the heat generation of MNPs under AMF. Enhanced tumor growth impediment has been shown by using doxorubicin release along with magnetic hyperthermia when compared to using either alone (more than a 7.5-fold reduction in tumor volume) [62].

3.1.1. Mechanism of heat generation using MNPs—Ferromagnetic materials are composed of multi-magnetic domains called Weiss domains. They can produce heat because of hysteresis loss during a magnetization cycle [63]. By applying AMF on the ferromagnetic materials, all the magnetic domains are forced to be parallel to the direction of the AMF to reach a lower energy state. When the AMF is removed, the magnetization does not come back to its original state (i.e. the state prior to the implementing magnetic field). To decrease the lingering magnetization, an opposite magnetic field (coercive field) is applied. The magnetization curve with a hysteresis loop in the ferromagnetic material is schematically shown in Figure 2a where Ms, Mr, and Hc present saturation, retentivity, and coercivity points, respectively. The area inside the hysteresis loop represents the hysteresis loss.

Superparamagnetism is a phenomenon that occurs in ferromagnetic NPs. Conventional bulk ferromagnetic materials consist of several magnetic domains while NPs are considered as

single magnetic domain particles because of their small size. They have a large magnetic moment that contains all atomic magnetic moments in the structure of the NPs. The superparamagnetic NPs have not shown any lingering magnetization after removing the AMF which makes them suitable for biomedical applications (Figure 2b). The power of MNPs to generate heat through exposure to an AMF is dependent on magnetization saturation (Ms), coercivity (Hc), and the frequency of the magnetic field [64].

The heat produced in ferromagnetic materials that are exposed to an AMF can be described by two different models: the relaxation (Néel and Brownian relaxations) and hysteresis loss.

The relaxing magnetism that occurs by quickly changing the orientation of magnetic moments (internal dynamics) is known as the Néel relaxation theory. This relaxation is prevented by an energy barrier (uniaxial anisotropy) which is accompanied by the heat formation in the ferromagnetic materials [65]. The relaxation time from this theory is determined by the equation below:

$$\tau_N=\tau_0\exp(\frac{KV}{K.b.T}), \quad (1)$$

Where $\tau_0=10^{-9}$ s, K is anisotropy constant, V presents the volume of the magnetic particle, k_b is Boltzmann constant, and T is the temperature (K). The size of NPs can strongly affect Néel relaxation.

The Brownian relaxation mechanism is explained by relative friction produced from the rotational diffusion of particles in a medium (external dynamics). In this theory, viscosity prevents the free rotation of NPs in the external medium [66]. Equation (2) gives the Brownian relaxation time:

$$\tau_B=(\frac{3\mu VH}{KB.T}), \quad (2)$$

here, μ, V_H, k_B, and T are the viscosity of the external medium, the volume of the particles, the Boltzmann constant, and the temperature, respectively. The size and viscosity are the most effective parameters in the Brownian relaxation theory [67]. The rotations of particles in a medium with higher viscosity are sluggish compared to a less viscous one. Generally, the Néel relaxation is the dominant force for small particles while the Brownian relaxation is the dominant one for large particles in the medium [65, 68]. Therefore, the relaxation of MNPs used in magnetic hyperthermia is primarily controlled with the Néel mechanism. The mixture of Néel and Brownian relaxation time yields the following equation [65]:

$$\tau=(\tau_B.\tau_N)/(\tau_B+\tau_N) \quad (3)$$

3.1.2. Delivery of MNPs to the tumor site—MNPs can be delivered locally via injection using catheters or hypodermic needles. MNPs can also be managed consistently and localized in the cancerous site by exposing them to an external magnetic field near the target tissue. In the direct injection method, magnetic fluid with a specific concentration of

MNPs is directly inserted into the cancerous tissue by injection. This method is the easiest approach because it does not require any further intervention for the particle localization. Therefore, the direct injection method is the most commonly employed approach in *in vivo* applications such as clinical studies [69]. Another advantage of direct injection is the controllability of the concentration of MNPs at the tumor site. However, this method is effective only when there is easy access to the tumor site. Additionally, MNPs tend to agglomerate post injection which negatively impacts their homogeneity within the tumor thus affecting the temperature distribution across the tumor. Accordingly, this approach is limited for many types of cancers [70]. In systematic delivery, the MNPs are intravenously injected. The concentration of MNPs increases in the bloodstream because of enhanced permeability and retention (EPR) effects [71]. Tumors have a faulty vascular architecture compared to healthy organs. Although the defective vasculature in tumor tissue can facilitate nutrient and oxygen supply for growing tumor cells, it can also result in easy penetration of macromolecules and NPs to the tumor site (Figure 3). Consequently, intravenous injection of NPs leads to their transport from the bloodstream to the cancerous area. Deposited NPs in a tumor have an extended retention time. The increased retention time is likely due to the ease of transportation of MNPs within the vasculature. The retention time and easy transportation of MNPs maintain stability and prevent agglomeration in the bloodstream. The diameter of particles used in systematic delivery is recommended to be less than 200 nm and higher than 50 nm to pass easily through the liver and survive renal clearance, respectively [72].

Saito *et al.* [73] revealed that coating NPs can significantly impact EPR retention. They coated superparamagnetic iron oxide with alkali-treated dextran magnetite (ATDM) and carboxymethyl dextran magnetite (CMDM). The ATDM coated IONPs showed more effective labeling of macrophages. The modification of protein adsorption and macrophages labeling of NPs can be achieved by using an effective and suitable coating for MNPs [74]. Although using the systematic delivery of MNPs results in a more homogenous distribution of particles at the tumor site compared to intratumoral injection, systematic delivery suffers from difficulty in providing the sufficient dosing of MNPs required for effective treatment. In addition, MNPs might accumulate in some healthy tissues.

To improve the localization of MNPs, they can be delivered to the tumor site through an active delivery approach. This way, the surface of MNPs is modified by a targeting agent that binds to cell receptors. By utilizing these interactions, higher concentrations of NPs and cellular uptake can be achieved in targeted tumor cells. These targeted agents can be antibodies [75], antibody fragments [76], receptor ligands [77], peptides [78], and aptamers [79]. Pala *et al.* [80] fabricated ferric oxide NPs with a dextran coating and human epidermal growth factor receptor (HER2) aptamer surface conjugate. The synthesized MNPs in their study were used as hyperthermia mediators. The results showed that the aptamer-tagged NPs specifically targeted HER2-expressing cells. Furthermore, a 90-fold lower dose of the tagged NPs was needed to attain ~50% cell death by hyperthermia treatment compared to that of the non-tagged NPs. The aggregation of MNPs in tumors could be optimized by controlling the external magnetic field [81]. Similarly, Dormer *et al.* [82] showed MNP guidance into the inner ear of guinea pigs by using an applied magnetic field with an optimized strength. In another study, AMF was used for passing MNPs through the blood-brain barrier and enable MNP penetration into the brain.

Overall, the active delivery of MNPs results in a better distribution of particles within the tumor site. However, identifying the correct targeting agent is vital to this technique but can be challenging depending on the phenotype of the cells in the tumor. The accessibility of the particles to the secondary tumors and metastatic regions is also not clear. In the case of multiple tumors, external magnetic fields are not able to be used to localize MNPs because there is mostly only one magnetic focal point for the direction of MNPs.

3.1.3. MNPs for hyperthermia-based therapy—There are various kinds of materials used for MNPs employed in hyperthermia therapeutics− namely Mn, Fe, Co, Ni, Zn, Gd, Mg, and their oxides. The applications of pure metals, despite having the high saturation magnetization, have been limited in biomedical engineering due to their instability in the human body and potential toxicity [83]. Metal oxides are more stable *in vivo* and exhibit higher biocompatibility than metals; thus, they are a more attractive candidate for medical applications [84]. Magnetite (Fe_3O_4) is a well-known magnetic material that can become stable by different ligands such as dextran [85], cationic liposomes [86], polyvinyl alcohol, hydrogel, and lauric acid [87]. Another group of MNPs is built upon ferrites, namely cobalt ferrites ($CoFe_2O_4$), manganese ferrite ($MnFe_2O_4$), nickel ferrite ($NiFe_2O_4$), and lithium ferrite ($Li_{0.5}Fe_{2.5}O_4$) [88]. Ferromagnetic NPs like doped Fe with Au and doped Zn/Mn with iron oxides ($Zn_xMn_{(1-x)}Fe_3O_4$) can be widely employed in hyperthermia applications [89]. FeCo metallic NPs have a high heating performance (1300–1600W/g) [90]. IONPs can be metabolized to produce blood hemoglobin and preserve iron cell homeostasis [91]. The chemistry, particle size, dispersity of NPs, and magnetic moment are the most important parameters in determining the hyperthermic strength of MNPs [92].

Chemical optimization of IONPs is of great importance in their application as a heat mediator in magnetic hyperthermia. Heat generation by the MNPs in hyperthermia applications can be described by three mechanisms: susceptibility loss, hysteresis loss, and viscous heating (magnetic stirring loss). Specific loss power (SLP) shows electromagnetic power loss per magnetic material mass and describes the magnetic strength of NPs. Recently, nano-ferrites have been extensively employed in hyperthermia applications because of their high SLP value. For example, bulk-shape of jacobsite and manganese iron oxide ($MnFe_2O_4$) has a higher SLP amount (110 emu/g) in comparison with bulk-shape magnetite (with SLP value of 92 emu/g). Spinels are a type of ferrites with the common formulation of MFe_2O_4 in which M is one of the divalent metal ions such as Mn^{2+}, Fe^{2+}, Co^{2+}, Ni^{2+}, Cu^{2+}, Zn^{2+}, Mg^{2+}, and Cd^{2+}. The dispersal of ions in the spinel structure is a key factor affecting their magnetization strength. In an inverse spinel structure, cations are placed in the octahedral sites in parallel to the magnetic field. Also, net magnetization strength is weakened by anions that are placed in tetrahedral sites. Doping MNPs with cations by desirable distribution in octal- and tetrahedral sites is an effective way of tuning their magnetic and physical properties with no effect on crystal structure [93].

Another important indicator in determining the heating power of MNPs is their size distribution. Gonzales-Weimuller *et al.* [94] studied the relation of SLP of monodisperse IONPs with their size. They found a direct relationship between SLP and the particle size wherein they measured the highest SLP (447 W/g at a field amplitude of 24.5 kA/m) for the NPs with a size of 11.2 nm. Their results also demonstrated that increasing the particle size

to ~12.5 nm results in higher heating rates. The size dependency of Fe_2O_3 NPs on generating heat in viscous media was investigated by De la Presa *et al.*[95]. They reported that the highest generated heat in viscous media can be achieved by having a critical MNP size of 12 nm. A key parameter in using MNPs as heat mediators in hyperthermia applications is their specific absorption rate (SAR). A low dosage of MNPs with high SAR value can generate a high amount of heat with lower magnetic field strength and frequency lowering the potential side effects.

Particle shape can potentially affect the performance of MNPs for heat generation in response to AMF. However, there is limited research on the influence of the shape of MNPs on heating properties. In one example, Song *et al.* [96] showed a strong relation of NP shape with their thermal efficiency. They prepared MNPs with two different shapes: spherical (average size of particle ~ 9.5 nm) and quasi-cubical (average size of particle ~ 9.6 nm) shape. The MNPs with quasi-cubical shape showed stronger saturation magnetization compared to the spherical-shaped particles.

Stabilizing the surface of NPs with a ligand agent leads to the improvement of their performance by decreasing toxicity, preventing agglomeration, and improving heating properties [96]. Pradhan *et al.* [97] synthesized MNPs with two different coating layers: lauric acid and dextran. Their results showed that lauric acid coatings can improve the cell-compatibility of MNPs more than dextran coating. Li Liu *et al.* [98] produced monodispersed Fe_3O_4 NPs coated with methoxy poly(ethylene glycol) (mPEG) to evaluate the effect of coated surface properties on the SAR under AMF. Their research showed a direct relationship between the thickness of coating and SAR where the SAR value decreases with reducing the thickness of the coated surface.

Achieving MNPs that can be suspended and that have suitable magnetization properties have recently been the matter of discussion for magnetic hyperthermia [99]. SAR is significantly affected by particle size, shape, and chemical composition of the MNPs. First, tuning the chemical composition of MNPs is an effective way of increasing the SAR value. Even though metallic magnetic nanoparticles have a good potential ability in enhancing SAR value [100], it has been reported that metallic particles are not stable at ambiance and using heavy metallic particles may cause toxicity [101]. It has been reported that SAR is strongly sensitive to the degree of colloidal stability and saturation magnetization [98]. Engineering MNPs with suitable shape and morphology without introducing any toxic material is of great importance in magnetic hyperthermia applications [99]. A unique magnetic structure can be achieved by engineering ferromagnetic vortex-domain nanorings (FVDNRs) with high SAR value, negligible remanence and coercivity, and good suspension ability [99]. Under an AMF, FVDNRs try to align with the field direction rapidly. FVDNRs are well-known for superior heat induction capability of the suspension that makes them an attractive mediated agent in hyperthermia treatment. In addition to FVDNRs, nanodiscs show much higher SAR value compared to isotropic particles [102]. It has been reported that parallel aligned nanodiscs under an applied AMF have ~2 times greater SAR value compared to randomly oriented nanodiscs [102]. Kim *et al.* showed that $Fe_{20}Ni_{80}$ microdiscs under the low-frequency magnetic field can be assumed as a strong thermal seed for destroying cancer cells [103]. MNP assembling is another important factor that has a significant role in the heating ability

of particles. Serantes *et al.* showed that chain-like arrangement biomimicking magnetotactic bacteria has good performancein magnetic hyperthermia applications [104]. The size of chains and anisotropy of particles in the chains have an important role in generating maximum heating [104]. The knowledge of tuning chemical composition, size, shape, morphology, and assembly of MNPs opens a new perspective for engineering strong MNPs in magnetic hyperthermia.

Strategies for engineering MNPs with high thermal energy transfer capability have been the focus of several recent research studies on hyperthermia and drug delivery methods [63, 105]. Lee *et al.* [106] took advantage of the exchange coupling between a magnetically hard core ($CoFe_2O_4$) and a magnetically soft shell ($MnFe_2O_4$) to improve SLP and enhance magnetic thermal induction of synthesized NPs. Their results showed that synthesized $CoFe_2O_4$@$MnFe_2O_4$ MNPs exhibit SLP values that are an order of magnitude larger than conventional IONPs. *In vivo* experiments were followed by subcutaneous injection of synthesized core-shell NPs into tumor tissue located in the abdomen of mice. An AMF of 500 kHz was applied for 10 min and the tumor size was monitored for up to one month. The tumors that received the hyperthermia treatment with $CoFe_2O_4$@$MnFe_2O_4$ MNPs were eliminated significantly. In summary, exchange-coupled MNPs can be developed as a new way of modulating magnetism for the enhancement of magnetic heat induction [106].

Janus particles are a relatively new class of heterogeneous particles that offer different properties in distinct regions. These particles can be designed to perform various functions without interfering with the functions of other regions or allow gradual exchange between the regions [107]. Liu *et al.* [108] developed Fe_3O_4 NPs-graphene oxide magnetic Janus amphiphilic nanoparticles (MJANPs) as high-performance NPs applicable in magnetic hyperthermia applications. Their results confirmed that developed MJANPs have magnetic heating efficiency and transverse relaxivity of 64 and 4 times higher than conventional IONPs, respectively. High-performance MJANPs can be extensively applied in different clinical diagnoses and therapeutic applications.

3.1.4. Self-regulated hyperthermia—A key concern in hyperthermia-based therapies is temperature overshoot. As the desired temperature tolerable by healthy tissue for such therapies is under 45 ºC [109], increasing temperature beyond can negatively affect non-cancerous tissues. Thus, finding methods for regulating the temperature and avoiding overheating is essential. MNPs immediately lose their magnetic properties when their temperatures reach the Curie temperature. Therefore, the saturation magnetization, Ms, becomes zero at the Curie temperature and no heat is produced when AMF is applied. It was reported that by choosing a suitable chemical composition and size of NPs, heating can be managed and overheating of surrounding tissue prevented [110]. Ni–Cu, Ni–Pd, and Co–Pd alloys are considered as top candidates for self-temperature regulating MNPs in hyperthermia therapy applications. Chatterjee *et al.* [60] synthesized polyethylene glycol coated copper-nickel NPs by the polyol reduction method and by a physical melting process. Their study showed that these NPs lose their magnetic properties in the range of 43–46ºC to control heat generation. Gd-substituted Mn–Zn ferrite NPs produced by the chemical co-precipitation method [111], $Fe_{1-x}Mn_xFe_2O_4$ NPs synthesized by the co-precipitation method

[112], and Fe-Pt, Ni-Pd, Ni-Pt NPs [113] have promising behavior in self-regulating MNPs in hyperthermia applications.

Apoptosis, an irreversible biological phenomenon, is the main agent of cancerous cell death when exposed to MNPs in an AMF. Magnetic hyperthermia is a favorable nominee for multimodal cancer treatments. In recent years, superparamagnetic iron oxide nanoparticles (SPIONs) have been broadly employed in hyperthermia therapy. Higher biocompatibility of SPIONs makes them more favorable in comparison with other magnetic materials, namely cobalt and nickel [114]. Using MNPs with high SAR value can generate high amounts of heat in lower strength magnetic fields and lead to fewer side effects. IONPs have superparamagnetic properties in particles with sizes of less than 12 nm [115]. At this size range, they have an extreme tendency for agglomeration. Coating SPIONs by a non-magnetic or magnetic shell is an alternate way to reduce aggregation phenomenon [115]. Overall, magnetic hyperthermia can be considered as an adjuvant to other techniques such as chemotherapy and drug delivery [54].

3.1.5. Hyperthermia combined with radiotherapy/chemotherapy—

Combinatorial hyperthermia treatment is the simultaneous or continuous exposure of cancerous tissue to thermal therapy along with another cancer treatment such as chemotherapy and/or radiotherapy. As mentioned, hyperthermia is not an effective treatment by itself. Hyperthermia in combination with radiation and chemotherapeutic agents has been carried out for years with significant improvement in the treatment of various types of cancers [116].

The combination of hyperthermia with chemotherapy and/or radiotherapy is categorized into three various types: thermo-radiotherapy, thermo-chemotherapy, and thermo-chemo-radiotherapy. One of the first examples of hyperthermia combination treatment was thermo-chemotherapy for the treatment of advanced liver melanoma metastases carried out in the early 1980s [117]. Even though the combination of hyperthermia with other cancer treatments has been developed in recent years, the combinatorial mechanisms are not fully understood and have remained a matter of discussion. Altogether, the benefits of using hyperthermia with chemotherapy and/or radiotherapy can be explained by the following synergistic effects:

- **a.** After cells are exposed to a specific dose of ionizing radiation, most cells go into synthesis phase (S phase), and simultaneous or continuous exposure of insensitive hypoxic cells to increasing temperature by hyperthermia therapy prevents DNA damage repair and increases treatment efficiency [118].
- **b.** Hyperthermia increases cell sensitivity to chemotherapeutic agents and enhances the uptake rate and accumulation of drugs in cancerous tissue [119].

A broad range of temperature elevations can be used in the hyperthermia method. For the best efficiency, a combination of moderate hyperthermia in the range of 42–45 ° C with chemotherapy and/or radiotherapy is preferred. It has been reported that the immune system response can be significantly activated within this range of temperature [16]. The combination of hyperthermia with chemotherapy and/or radiotherapy has been reported for

the treatment of colorectal cancer [120], prostate cancer [121], bladder cancer [122], cervical cancer [123], and peritoneal carcinomas [124].

While most of the MNPs used in hyperthermia therapy can be employed in the combination of hyperthermia therapy/radiotherapy/chemotherapy, gold nanoshells have been reported as an adjuvant to improve the efficacy of thermal therapy in combination with radiotherapy and chemotherapy [125] because of their unique optical, electrical, and drug loading capacities [126]. MNPs integrated with chemotherapeutic agents can simultaneously release drugs and selectively transfer heat to tumor cells. Combining hyperthermia with radiotherapy and chemotherapy using MNPs suggests high cancerous tissue penetration, selective tumor targeting, decreased toxicity effects, and improved therapeutic response.

3.2. Drug delivery vehicles

Each type of cancer requires a specific method of treatment due to the vast differences in the large array of potential cancers and specific differences in each patient. Conventional chemotherapy has several disadvantages including nonspecific distribution of drugs in tumors and healthy tissues, rapid clearance of anti-cancer agents, significant toxicity of anti-cancer drugs for normal tissues, and difficulty of choosing a suitable dose of drugs in the cancer treatment [127]. Consequently, understanding the molecular and cellular reactions of different types of cancers and designing the specific drugs to treat them have recently drawn noticeable consideration [128].

Based on these studies, various types of drug vehicles like polymeric NPs and micelles, liposomes, carbon nanotubes, graphene oxide, MNPs, and silica and gold NPs with unique properties have been developed for overcoming barriers preventing effective delivery of drugs into cancerous tumors [28]. The hydrophobic properties of most drugs reduce their bioavailability within the bloodstream. One of the advantages of encapsulating drugs in a polymer structure is to improve their bioavailability in the body. These modifications can control drug release at the tumor site over time [129].

One promising approach that has been widely studied is to engineer drug carriers that respond to external stimuli [130]. Two classes of particles have received particular attention: infrared (IR) responsive drug carriers and MNP-based drug carriers. The key advantage of MNPs over IR responsive drug carriers is the ability of MNPs to be localized by employing external magnetic fields prior to their activation. In addition, MNPs can combine both hyperthermia therapy and sustained drug release.

3.2.1. Types of utilized drugs—The unique properties of MNPs make them attractive candidates for drug delivery, diagnosis, and treatments of cancers [131]. Radiolabeling is a well-developed and helpful method for quantitating biological uptake [132]. Positron emission tomography (PET) or single-photon emission computed tomography (SPECT) are highly-developed diagnostic methods relying on positron emitters nanomaterials [133]. Both cancerous tissues and biological phenomena are distinguishable using radiolabeled MNPs. Recently, alpha- and beta-emitter-labeled NPs have been extensively investigated for clinical applications and some trials have presented excellent results on tumor treatment [134]. Altogether, biomolecules such as antibodies, peptides, and aptamer and small-molecule

drugs can be labeled with MNPs for the best diagnosis and treatment of cancers. The incorporation of various radionuclides on the surface of MNPs results in transporting alpha- and beta-emitters to the cancerous tissues. Furthermore, MNPs can be labeled with different functional molecules like cancer-targeting molecules such as antibodies, peptides, and molecule ligands [135]. This strategy leads to the development of multivalent MNPs applicable in cancer therapy and diagnosis (Figure 4).

3.2.1.1. Chemotherapeutics: Chemotherapeutics, which are primarily small organic drugs, kill cells that undergo rapid mitoses such as cancer cells, bone marrow, and hair follicles [136]. Systematic chemotherapy, without controlled release, has several side effects such as immunosuppression (myelosuppression), inflammation of the lining of the digestive tract (mucositis), and hair loss (alopecia) [137]. But, their delivery to the targeted tumor by MNPs can remove these unwanted side effects [138].

Kohler *et al.* [139] synthesized methotrexate-immobilized IONPs as a drug vehicle. They conjugated synthesized NPs with methotrexate (MTX)−a chemotherapy drug−by poly (ethylene glycol) (PEG) self-assembled monolayer. NP-PEG-MTX shows higher cytotoxicity in 9L glioma cells than free MTX *in vitro*. Hua *et al.* [140] developed a nontoxic drug nanocarrier in a core/shell form that encapsulated paclitaxel (PTX). Their results showed that synthesized nanocarrier-bound-PTX has higher stability compared with free-PTX under the studied conditions. Additionally, the bound-PTX nanocarrier is more toxic to human prostate carcinoma cells (PC3 and CWR22R) compared with free-PTX, especially under AMF.

3.2.1.2. Radiotherapeutics: Modern cancer therapies have been partially successful at treating many common types of cancer and prolonging the lives of patients [141]. For instance, radiotherapeutics can destroy cancer cells by damaging the DNA of cancerous cells through the generation of free radicals. Recently, different targeting systems including MNPs conjugated with antibodies and peptides have been developed to support direct radionuclides away from non-cancerous sites, paralleling chemotherapeutic development [142]. This kind of treatment is different from conventional drug delivery tools and can act at a distance of nanometers to microns from the tumor site. ß-emitters (as radionuclides) can attach to different radionuclide labeled MNPs (such as ^{188}Re [143] and ^{111}In [144]) to be used as therapeutic agents for treating cancer cells.

3.2.1.3. Antibodies and peptides: Antibodies can target certain antigens specifically expressed or overexpressed on cancer cells. Scientists can design and rapidly replicate monoclonal antibodies (mAbs) to target cancerous tissues. Ross *et al.* [145] prepared Herceptin (commercially marketed as Trastuzumab) conjugated IONPs as heating mediates for hyperthermia applications and as an agent in controlled drug release for breast cancer treatment. They reported that the combination of MNPs and Herceptin significantly increases their ability to kill Her2/neu expressing breast cancer cells.

Peptides are molecules with amino acids linked by peptide bonds through the dehydration-condensation reaction. Veiseh *et al.* [146] synthesized a nano-system vehicle−amine-functionalized PEG silane conjugated superparamagnetic iron oxide−for the delivery of a

peptide, chlorotoxin (a natural amino acid identified from the venom of a scorpion to diagnose glioma and prevent tumor invasion, CTX). Their results showed a more than a two-fold improvement of the cancer invasion inhibition rate by binding CTX to the surface of synthesized NPs. Figure 5a represents the mechanism of inhibiting tumor cell invasion by NP-PEG-CTX. Figure 5a also shows that the nano-system carrier is composed of IONPs as the core, PEG polymer as an agent for increasing biocompatibility and ligand binding sites, and CTX as the peptide. A necessary component for glioma cell invasion is the MMP-2 endopeptidase complex. The synthesized NPCs prevent the activity of the MMP-2 endopeptidase and result in limiting cell invasive activities.

3.2.1.4. Oligonucleotides: Oligonucleotides are short DNA or RNA molecules, oligomers, with numerous applications in various fields, especially in genetic research [147]. Gene therapy is one of the most suitable methods for treating inherited diseases. This method has many limitations such as biocompatibility of viral vectors along with the unsatisfactory *in vivo* efficiency of non-viral vectors [148]. Attaching nucleic acids to MNPs could potentially overcome these limitations. Most researchers use cationic polymers such as PEI and polyamidoamine to make a bond between MNPs and nucleic acids [149]. The ionic bonding between cationic polymers and nucleic acids can protect the nucleic acids against enzymatic degradation. Medarova *et al.* [150] developed an adeno-associated virus (AAV) attached to magnetic microspheres. They showed that these complex microspheres can increase the transduction efficiency both *in vitro* and *in vivo*.

3.2.2. Remote controlled pulsatile drug release—On-demand release systems have drawn significant attention for the treatment of various diseases as they potentially allow the delivery of the correct drug quantity at the correct time [151]. Pulsatile release of drugs can be caused by either specific molecules around drug-loaded systems or applied specific stimuli from outside of the body [152]. Responsive materials are a class of materials that react to specific changes in the surrounding environment [153]. A combination of MNPs in a responsive hydrogel matrix can present unique properties such as the ability of actuation from outside of the body by light or magnetic field. These systems can show an on-off, switchable drug release using external AMF control. A combination of inorganic materials such as MNPs in the polymer network will affect intrinsic characteristics of the polymer substrate such as mechanical properties and gelation time [154].

Firstly, Langer et al. developed a controlled on-demand insulin release system composed of ethylene vinyl acetate and embedded magnets [155]. Gao et al. developed ferromagnetic vortex-domain iron oxide (FVIO) combined into chitosan hydrogel by the grafting-onto technique [156]. Their results showed that a 17-fold lower concentration of FVIOs (0.6 mg/mL) is needed compared to SPIOs (10mg/mL) for reaching the same heat-inductive effect. *In vivo* experiments showed that their magnetic hydrogel significantly improved efficiency of chemo-thermotherapy technique and could extremely kill residual cancer cells and arrest breast cancer cell proliferation. Such on-demand therapeutic release systems can potentially overcome the limitation of conventional SPIOs and drug-containing hydrogel systems because of their high inductive heating capability [156].

3.2.3. Multifunctional magnetic nano-systems for hyperthermia and drug delivery applications—By using hyperthermia treatments and chemotherapy simultaneously, the effectiveness of the therapy can be improved. Recently, pH-sensitive and thermal-responsive nanocarriers have been implemented in drug delivery and placed under AMF. Among these multifunctional systems, polymeric carriers, polymeric core/shell NPs, liposomes, and micelles have attracted the most attention in the field of cancer therapy. Generally, NPs used in thermo-chemotherapy applications are synthesized from inorganic metals and ceramics, organic polymers and lipids, and organic/inorganic hybrid NPs; therefore, they can be classified as reported in Figure 5b. Here we discuss important magnetic nano-systems for application in thermo-chemotherapy.

3.2.3.1. Core/shell MNPs: A wide range of studies has focused on developing MNPs encapsulated in polymeric NPs for hyperthermia and drug delivery applications [15]. By using polymeric NPs, the shape, size, surface charge, biocompatibility, and structure can be tailored.

Core-shell NPs with a magnetic core and organic polymer shell loaded with drugs have dual applications in hyperthermia and drug delivery. By using this system, the biocompatibility, conjugation with other bioactive molecules, circulation time in the bloodstream, and thermal/chemical stability can be significantly improved while simultaneously reducing agglomeration [157].

Polymers can be stuck to the surface of MNPs by two mechanisms [158]. The first method is called “grafting to”, where an end-functionalized polymer is directly attached to the surface of the NPs. The second mechanism, “grafting from,” is where the polymerization initiates from the surface of MNPs by an initiator. The polymer can also attach to the surface of NPs by non-covalent interactions, such as electrostatic or Van der Waals interactions.

In one study, Taratula *et al.* [37] synthesized a multifunctional tumor-targeting delivery system with IONPs as a core (for mild hyperthermia) and polyethylene glycol and Luteinizing hormone-releasing hormone (LHRH) peptide as a shell (for loading doxorubicin, improving biocompatibility and tumor target acquisition). Their synthesized core/shell system presents a relatively uniform size distribution of NPs without agglomeration (Figure 6a). The TEM image shows that the iron oxide core has a diameter of 27.7 nm with a shell thickness of 8.7 nm. This size range for both the core and shell of NPs makes them favorable for cancer therapy. Due to their small size, nanoparticles can pass through various physical barriers and penetrate into cancer cells [159]. A faster drug release from the nanocarrier was achieved in acidic conditions (a tumor-like environment) (Figure 6b). The magnetic iron oxide core produced heat after exposure to an AMF, where the heat was managed by turning the field on and off (Figure 6c). Their results confirmed that the simultaneous use of chemotherapeutic drug and mild hyperthermia leads to more than 95% cancerous cell death *in vitro* (Figure 6d).

3.2.3.2. Liposome/magnetic nanoparticles hybrid nanoparticles: A liposome is a vehicle with a spherical shape consisting of at least one lipid bilayer and an aqueous core. The liposome is used as a vehicle for carrying nutrients and drugs [160]. For instance,

researchers can attach hydrophilic chemotherapeutic drugs to the aqueous section of the liposome or encapsulate hydrophobic drugs in the lipid membrane. Drug delivery by liposome can protect and increase the circulation time of drugs in the bloodstream and prevent drug removal via renal filtration and reticuloendothelial system that results in increasing deposited drugs in the cancerous site through the influence of EPR [161]. MNPs can be incorporated into the drug-filled liposomes, either in aqueous core [162] or in the lipid membrane [163], to form magnetoliposomes. Using a temperature-sensitive polymer in the lipid layer can make smart liposomes that release drugs as temperature increases.

Employing a thermo-responsive polymer in liposome structure can result in a smart drug release carrier. Temperature-sensitive polymers have a phase transition temperature and critical solution temperature (CST). Under this critical temperature, drugs are retained within the liposomes and are released when the temperature increases; this is accomplished by disrupting the lipid bilayer through their sensitive solubility in water with respect to the temperature [164]. At a temperature lower and higher than CST, the structures are soluble and insoluble in water, respectively, which results in efficient drug release [165]. Poly (Nisopropylacrylamide) (pNIPAAm), highly temperature-sensitive, is considered amongst the most attractive polymers for drug delivery systems due to its LCST of 32 ˚C in water. Stoychev *et al.* [166] revealed that the LCST of pNIPAAm is able to be altered by using different ratios of hydrophilic/hydrophobic co-monomers. By tuning LCST in the range of employed temperatures in hyperthermia therapy, the drug can be maintained in the polymer structure until hyperthermia temperatures induce drug release. The pH-sensitive polymers can also be used for smart drug delivery. The pH changes based on the location in the body and the type of tissue. The pH is more acidic in the cancerous site than in a healthy site. Liposomes as pH-sensitive drug delivery systems can be used to release a payload of drugs at a specific pH value.

Qui *et al.* [167] developed a magnetoliposome with SIONPs embedded in a membrane. They employed the supercritical carbon dioxide method for synthesizing their particles. Their experiments showed that the payload within liposomes can be controlled released when exposed to AMF (Figure 7a and b). The ability to control drug release allows for improved cancer treatment due to increasing control of dosages, site specific release and time of release. The ability to control drug release allows for improved cancer treatment due to increasing control of dosages, site specific release, and time of release.

3.2.3.3. Micelles: Micelles are lipid molecules that self-assemble into spherical form in aqueous solutions. They contain a hydrophilic head and a hydrophobic tail. They have a core/shell structure formed by amphiphilic block copolymers [168]. Generally, they have both hydrophilic and hydrophobic properties due to the polar head groups and the long hydrophobic chain structures, respectively. Hydrophobic drugs are encapsulated within the hydrophobic core of the micelles. Micelles have numerous advantages in drug delivery applications because of their ability to increase factor circulation time in bloodstream, enhancing drug deposition through the EPR influence in cancerous tissue, and protecting drugs from clearance by the renal and reticuloendothelial processes. Micelles, similar to the liposomes, have the ability to become sensitive to temperature by coupling them to thermo-responsive polymers in the head or tail section [169].

Kim *et al.* [39] synthesized poly (N -isopropylacrylamide-co-acrylamide)-block-poly (ε-caprolactone) random block copolymer micelles with a multifunctional thermo-responsive property for magnetic hyperthermia-mediated payload release of doxorubicin (DOX). They added IONPs (11 nm in diameter) in the synthesized micelles where the diameter of the SPION-loaded micelles and their LCST were ~70 nm and ~43˚C, respectively. The topographic atomic force microscope image and TEM images from their synthesized micelles are presented in Figure 7c and d. For comparison, they measured DOX release from micelles in two different modes: in a water bath and magnetically induced heating. Their results showed that the magnetically induced heating leads to a three-time increased released of DOX at 43° C compared with the water bath (Figure 7e).

Photodynamic therapy (PDT), as a multifunctional diagnosis and treatment method, has been extensively developed in the past decades. In this method, photosensitizers (PS) are irradiated using a specific wavelength of light resulting in the formation of toxic singlet oxygen (SO) that kills cancer cells [170]. To achieve the best efficiency of PDT, several challenges need to be overcome. First, some PSs are insoluble and have a tendency to agglomerate in an aqueous media. Second, single-modality imaging cannot provide more specific information in a practical clinical application. Third, developing suitable carriers for high PS loading is challenging and has been of major focus in recent years. One way to overcome these problems is the delivery of PSs by different nanocarriers such as micelles [171], liposomes [172], MNPs [173], and quantum dots [174] for diagnostic imaging and PDT. Even though these carriers meet some requirements for a high delivery of PSs, there are still several limitations that need to be solved.

4. Cancer Diagnosis

4.1. Imaging

Medical imaging is often employed to study biological phenomena, detect abnormalities, and monitor the progress of diseases [174]. State of art techniques for imaging is constantly being developed to improve the resolution of medical images. These techniques include magnetic resonance imaging (MRI), positron emission tomography (PET), computed tomography (CT) and single-photon emission computed tomography (SPECT), optical fluorescence imaging, ultrasound (US) imaging, and photoacoustic (PA) imaging [175].

MRI employs strong magnetic fields and radio waves to take a picture of specific organs and tissues [176]. Often, MRI is the best choice due to its accuracy, the ability to produce 3D images, excellent spatial resolution, providing good contrast with soft tissue, excellent signal-to-noise-ratios, and the lack of harmful radiation. However, it has some disadvantages such as long processing times and the large capacity of the generated data [177].

CT is an X-Ray based technique to create detailed images of internal organs, bones, soft tissue, and blood vessels [178]. Ionizing radiation (X-Ray) is an important disadvantage of the CT method [179].

A PET scan uses a nuclear technique for imaging. This technique provides insight into movement and absorption of chemicals into specific tissues to diagnose diseases [180]. This

method is built upon the detection of emitted pairs of gamma rays by a positron-emitting radionuclide in a biologically active molecule. The use of ionizing radiation (Gamma and Beta rays) is considered as the main disadvantage of this method. Beyond its disadvantages, a PET scan has great superiority in its ability to detect cancerous and non-cancerous tissues in early stages of growth, a lower probability of infection from medical procedures, and a more effective ability to diagnose early stages of some neurological illnesses like Alzheimer's disease [181].

SPECT is a nuclear medicine tomographic picturing method that also works with gamma rays [182]. This technique is the same as conventional CT imaging except this method is working with the detection of nuclear energy using a gamma camera. For this reason, a gamma-emitting radioisotope material (such as an isotope of gallium (III)) is introduced into the bloodstream. Usually, the radioisotopes are attached to a specific ligand to make a radioligand, and this ligand binds to tissues of interest. This attachment allows the combination of ligand and radiopharmaceutical to be delivered and bound to the desired place in the body, where the ligand concentration is seen by a gamma camera. Like CT and PET techniques, ionizing radiation (Gamma-Ray) has the same issues of radiation exposure due to employing gamma rays [183].

High contrast images of small biological tissues in complex environments is an important tool for disease identification. For this reason, recent developments have been made to enhance these techniques. One of the most attractive methods is using multimodality imaging to eliminate the disadvantage of a single imaging modality. Using imaging agents such as MNPs overcomes inherent instrument and machine limitations and can work as contrast agents to meet the requirements of the imaging process.

4.1.1. MRI contrast agents—MRI is an attractive imaging method and a powerful cancer diagnosis tool that has excellent abilities such as high contrast in imaging soft tissue, high spatial resolution [184], and less radiation exposure in comparison to CT and PET [185]. The principles of MRI and nuclear magnetic resonance (NMR) are the same. In this technique, a strong magnetic field is applied to a patient or specimen where the orientation of hydrogen nuclear spin is in the same or opposite direction of the applied magnetic field to obtain a lower or higher energy state, respectively. Irradiation of resonant radiofrequency results in the absorption of energy by the nucleus and increases the number of the spin to a higher-energy state (the opposite direction compared to the applied magnetic field) which leads to a non-equilibrium state. Therefore, the excited nuclei reduce their energy state to reach equilibrium or relaxation state by emitting a weak but detectable radiofrequency. Several atoms can be used for the magnetic resonance signal, but hydrogen nuclei located in the desired site are usually identified to make a cross-sectional magnetic resonance image. Increasing the magnetic field strength can lead to improved contrast, sensitivity, and resolution of MR images. However, increasing the magnetic field strength increases the power of the radiofrequency. Due to the radiofrequency energy that is absorbed in the body of the patient, the radiofrequency emission can result in increased body temperature. Therefore, for MRI techniques in biomedical applications, the most common magnetic field strength ranges from 1.5–3 T.

Protons of ^{1}H, ^{11}B, ^{19}F, ^{13}C, and ^{31}P atoms that are prevalent in molecules that compose tissues can be used as a source for the MRI signal. Of all protons, hydrogen (^{1}H) is employed as a primary source of MRI signal due to high availability in tissues [186]. There have been two main relaxation processes used in MRI including longitudinal (spin−lattice relaxation) and transverse relaxation (spin−spin relaxation) [187]. Switching off the external magnetic field (B_0) returns the excited protons to the lower energy state (equilibrium or relaxation state). The longitudinal magnetization of protons recovers slowly (longitudinal relaxation). T_1 is the relaxation time for recovering longitudinal magnetization from zero to 63% of pre-magnetization levels [188]. The proton simultaneously and independently spins with a Larmor frequency of $\omega_0 = \gamma B_0$ (where γ is the gyromagnetic constant). By implementing a radiofrequency pulse of ω_0, the direction of proton nuclear spins becomes the opposite direction of B_0, and by decreasing the longitudinal magnetization, transverse magnetization is produced. Upon removing radiofrequency pulse, the excited water protons return to their relaxed state (parallel to the direction of B_0). During this process, the protons emit the observed energy from the RF pulse. The needed time for lowering the magnetization from a maximum value to 37% (1/e) of its excited state is called T_2. T_2 presents the decaying or dephasing of transverse components of magnetization [188].

The principle of contrast agents in MRI techniques is based on T_1 (longitudinal relaxation) and T_2 (transverse relaxation). Generally, these relaxation processes can be recorded and modified into grayscale images. MR contrast agents improve contrast by reducing the MR relaxation times and can affect T_1 and T_2 by dipole-dipole interactions [189]. The rate of longitudinal magnetization recovery and transverse magnetization decay can be evaluated by r_1 (the inverse of T_1) and r_2 (the inverse of T_2), respectively. In T_1-weighted mode in MR images, T_1 relaxation time is short and longitudinal magnetization is recovered fast. In this condition, tissue appears bright. Oppositely, in T_2-weighted mode in MR images, targeted tissue quickly loses its transverse magnetization and appears dark. MR is primarily dependent on the changing of local proton relaxation times, which is extremely influenced by the water content of tissues and the ability of hydrogen molecules to move. There are different water proton densities in various tissues. This issue has a strong influence on the rate of water proton relaxation and can lead to depict recognizable MRI contrasts in different biological tissues [190].

In clinical applications, the highest resolution images are created using T_1 because it produces a bright signal. Dark signals created by T_2 can be confused with interior conditions like air, hemorrhage, and blood clots [191]. Paramagnetic ions near the protons can affect T_1 contrast agents. Gd^{3+} with seven unpaired electrons has the best effect. Gd-diethylenetriaminepentaacetic acid (Gd-DTPA) and tetraazacyclododecanetetraacetic acid (Gd-DOTA) are primarily only employed in clinical applications due to the toxicity of free Gd^{3+} [192]. Additionally, Gd^{3+} causes side effects like nephrogenic system fibrosis [193]. For this reason, Mn^{2+} compounds have been developed [194]. However, their biocompatibility has not been fully assessed, and they can induce side effects such as neurotoxicity [195]. SPIONs are attractive agents to improve contrast and clarification. They have shown high biocompatibility and lower probability of rejection [196].

The ability to accelerate relaxation rates is described by relaxivity coefficients (r_2 or r_1 ($mM^{-1}S^{-1}$)). To achieve the optimum T_2 MR image contrast, high r_2 values are preferred (high r_2/r_1 ratio). Compared to T_2, T_1 MR image contrast should show a high r_1 value (low r_2/r_1 value). Selecting suitable MNPs can affect T_1 and T_2 MRI contrast agents and optimize the r_2/r_1 value. Size, composition, surface state, and shape of MNPs are considered as the important parameters in adjusting r_2/r_1 ratio (Figure 8a).

4.1.1.1. Size: Since the electrical properties of atoms on the surface of MNPs are completely different from those located in the inner surfaces, the total magnetic moment of MNPs is an integrated sum of magnetic spins on the boundaries and at the center of MNPs [27b]. Several studies have shown that saturated magnetization (M_s) and diameter (r) affect T_2 relaxation enhancement [197].

MNPs with larger sized diameter have higher M_s values [198]. Cheon et al. reported Ms values of 25, 43, 80, and 102 emu.g iron for IONPs with the diameter size of 4, 6, 9, and 12 nm, respectively [198]. Smaller sized MNPs expose a higher number of metal atoms on the surface for water proton proportion and chemical exchanges [27b]. Lu *et al.* showed that small-sized IONPs are effective T_1 contrast agents for achieving high-resolution MR angiography in beagle dogs [199].

Kim *et al.* [200] demonstrated that the particle size has a significant impact on the magnetic properties of MNPs. They synthesized homogenous extremely small iron oxide nanoparticles (ESIONs) with different diameter sizes (1.5, 2.2, 3, and 12 nm). The magnetization of synthesized ESIONs tended to decrease by reducing the particle size (Figure 8b). The spin canting effect states that the spins of surface atoms possess are never fully aligned. If it is assumed that the spin canting layer of iron oxide particles is 0.8 nm, 93.6% of spins in 3 nm-sized IONPs will be canted. For the IONPs with the diameter of 12 and 2.2 nm, 38.6% and 99.4% of spins are canted, respectively (Figure 8c). The magnetic moment per particle sharply decreases when particle size reduces. As Figure 8d shows, after injection of 12 nm-sized ESIONs into a rat via its tail vein, blood vessels are more visible on the T_1 weighted MRI showing that ESIONs are able to improve T_1 relaxation in the circulation system.

4.1.1.2. Composition: Composition of NPs affects their total magnetism and, therefore, their role in MRI contrast agents [201]. The magnetic strength of NPs is influenced by the introduction and distribution of metal dopants in the structure of NPs. The position of iron ions in octahedral or tetrahedral sites of MNPs affects its magnetic strength [202]. The iron ions in octahedral sites of magnetite structure induce ferromagnetic properties while the magnetic ions in tetrahedral sites are in an anti-ferromagnetic position. Since there are equal amounts of iron ions in octahedral and tetrahedral sites within the magnetite structure, their magnetic spins neutralize each other. One way to tune magnetic strength of MNPs is doping iron ions with other transition metal ions such as Co^{2+}, Mn^{2+}, Zn^{2+}, and Ni^{2+} and, thus, make magnetism-engineered iron oxide (MEIO) NPs (MFe_2O_4, M = Ni, Co, Fe, and Mn) [203]. By doping iron ions in a magnetite structure with Ni, Co, and Mn, the saturation magnetization (M_s) value becomes 85, 99, and 110 emu/g and the r_2 value is 152, 172, and 358 $mM^{-1}s^{-1}$, respectively.

Zho *et al.* [41] showed that T_1 contrast effects are improved when a rare-earth element (such as gadolinium) is doped in IONPs. They synthesized gadolinium-embedded iron oxide (GdIO) NPs and evaluated the doping effect on T_1 MRI contrast. They showed that by embedding gadolinium in IONPs, the interior spins of NPs are dispersed, and the thickness of the spin canted layer is increased. This behavior can strongly affect T_1 MR image contrast and improve image brightness (Figure 9a). They also investigated *in vivo* T_1 MRI of mice after injection of 4.8 nm gadolinium-embedded iron oxide of a 2.0 mg (GdIO)/kg (mice) dose at various time periods (0, 10, 30 and 60 min) (Figure 9b). As can be seen, injecting GdIO NPs enhances the contrast of images from the heart, kidneys, and bladder at 10 min following injection. A decreasing signal can be visible in the heart while the increasing signal has been observed for kidneys and bladder over time.

Physical-vapor-infiltration was employed for synthesizing mesoporous silica nanoparticles (MSNs) embedded with USPIO NPs [204]. Due to the unique metal-ligand coordination bonding between the Fe species and anticancer drug molecules, the synthesized MSNs-IONPs were employed to simultaneously improve T_1 MRI contrast and as a ground for the loading and stimuli-responsive release of anti-cancer drugs. It was believed that the bonding between Fe and drugs encapsulated within the mesopores would be stable under physiological conditions because iron species and protons were Lewis acids, whereas DOX was a Lewis base. Therefore, a synthesized MSNs-iron oxide system could act as a pH-sensitive drug releasing system. *In vivo* MRI tests were done by inserting MSNs-IONPs inside mice and MR images were recorded at different time intervals (Figure 10a). The T_1-weighted images indicated that the positive signal intensities in cancerous tissue greatly improve after the injection of an MSNs-iron oxide nano-system. T_2-weighted images did not reveal considerable improvement following injection. The *in vitro* DOX drug release showed that releasing DOX drugs from an MSNs-iron oxide system was strongly dependent on pH (Figure 10b). Under neutral conditions (normal physiological human body), only 14.4% of the DOX drug was released in 24 hours, while by decreasing the pH value to 4 (pH near cancer tissue), DOX release reached 67.2%. The *in vivo* MRI experiments were followed by injection of MSNs-DOX-IONPs inside mice and then were subjected to MR imaging at different time intervals (Figure 10c). After the injection of MSNs-DOX-IONPs, a decreasing pH value near the cancer tissue induces the cleavage of the bonds between Fe and the drug. This decreasing pH value exposed the Fe paramagnetic centers to water molecules. Therefore, releasing the drug from MSNs-IONPs improved the intensity of T_1-weighted MR images (Figure 10c).

Ultrasmall ferrite nanoparticles (UFNPs)-based T_1 contrast agents have been extensively used, in recent years, for reaching to high-resolution MR images [199, 205]. Compared to the Gd-based T_1 contrast agent, UFNPs with sizes smaller than 5 nm present a higher T_1 MR value [206] and lower toxicology level [207]. Among UFNPs, ultrasmall manganese ferrite nanoparticles (UMFNPs) have been shown to have elevated r_1 relaxivity value (up to 1.7 times higher) compared to maghemite NPs of the same sizes [208]. UMFNPs (with chemical formula of $Mn_xFe_{3-x}O_4$) have the highest and lowest T_1 relaxivity at $x = 0.75$ and $x = 1.57$, respectively [209]. However, increasing manganese doping content to $x>1$ has a significant adverse impact on the biocompatibility. High release of Mn^{2+} may potentially induce

toxicity that should be optimized. Recent studies have shown that $Mn_xFe_{3-x}O_4$ (x = 0.75–1) NPs presents optimal T_1 MR value and biocompatibility [208].

4.1.1.3. Surface characteristics: As it was mentioned in the proceeding section, a coating that provides increased biocompatibility with suitable thickness around MNPs can lower toxicity, increase circulation time, decrease agglomeration, and modify drug release abilities [210]. However, this type of coating can also affect the r_2/r_1 value. Polyethylene glycol (PEG) coated IONPs have been prepared for use as contrast agents in T_1 MR images by Tromsdorf *et al.* [211]. They showed that the r_1 value is not dependent on the chain length of PEG, while r_2 is strongly dependent on the PEG chain. Schwaminger *et al.* [212] confirmed that the oxidation layer reduces magnetization and strongly effect charge, reactivity, biocompatibility and catalytic properties of IONPs.

4.1.1.4. Assembly: The assembly of superparamagnetic NPs strongly affects the contrast of T_2 MR images [213]. NPs have a high tendency to agglomerate and cluster. Each cluster is composed of several MNPs that are assumed to be a single large magnetized sphere, and its total magnetic moment has a direct relationship with its size (the number of NPs inside the cluster). Poselt *et al.* [214] synthesized PEG-coated IONPs for contrast agents in T_2 MR images. They synthesized four differently sized NP clusters with different hydrodynamic diameters of 51, 70, 79, and 141 nm (Figure 11a). They employed dynamic light scattering (DLS) measurements to obtain hydrodynamic diameters (d_{hyd}) (Figure 11b). Transverse relaxivity, r_2, is sensitive to the diffusion length of water molecules into the particles. The transverse relaxivity of NP clusters showed three different regimes dependent on cluster size: the motional averaging regime (MAR), the static dephasing regime (SDR), and the echo-limiting regime (ELR). The value of r_2 increased in the MAR region, stayed constant in the SDR region, and decreased in the ELR region (Figure 11c). The best value of r_2 was obtained in the SDR region where the size of IONPs clusters was around 100 nm. Therefore, controlling the agglomeration of NPs was important for obtaining maximum r_2 relaxivity [215].

While most MNPs have a high tendency to localize at diseased tissues, conjugation with affinity ligands−such as antibodies, peptides, and aptamers−is of great importance in their detection ability. MNPs decorated with ligands accumulate in cancer cells and generate significantly higher MR signals compared to those without ligands [216]. It is widely accepted that the T_2 relaxivity values of MNPs are strongly dependent on ligands attached to their surfaces [216]. Covarrubias *et al.* [217] decorated IONPs with two different kinds of ligands targeting two different upregulated biomarkers on the tumor endothelium, P-selectin and fibronectin for focusing and imaging of breast cancer in mouse models. They showed that single-ligand nanochain attached IONPs have a 2.5-fold higher intratumorally adhesion compared with IONPs. MR signals generated by IONPs conjugated by affinity ligands showed more detectable MR signals.

The sensitivity and contrast of MRI could be improved by contrast agents like MNPs. While plenty of isotopes are employed as MRI contrast agents (such as ^{7}Li, ^{13}C, ^{83}Kr, etc.), the dominant approach in MRI is based on the hydrogen content from water in the human body [218]. By applying an electromotive force (EMF), the magnetic moments of hydrogen nuclei

are forced to align in the orientation of the magnetic field and a radiofrequency is generated. After removing radiofrequency perturbation, the hydrogen nuclei try to come back to their initial state at the original equilibrium by relaxation process [219]. The rates of relaxations are determined by longitudinal relaxation time (T_1) and the transverse relaxation time (T_2). In order to improve image quality in an MRI, the relaxation process should be accelerated. Recently, Gd chelates and IONPs are synthesized as clinical contrast agents of T_1 and T_2, respectively. However, several types of researches have improved contrast agents with higher increased contrast potential. The most important properties of MNPs affecting their magnetism and contrast effect are their size, composition, and assembly. It was found that the strength of magnetism is improved by decreasing the size of NPs. The introduction and distribution of metal dopants such as Co^{2+}, Mn^{2+}, Zn^{2+}, and Ni^{2+} in NPs structure can affect their magnetic properties. T_1 and T_2 contrast agents can produce bright and dark signals. Applying T_1-weighted or T_2-weighted MR images causes the loss of some detail from diseased tissue. In the next section, T_1–T_2 dual-mode MRI contrast agents that present valuable information from unhealthy tissues, with special focus on cancer tissues, will be discussed.

4.1.1.5. Shape: The strong and separate parts of MNPs are magnetic moments that are affected strongly by the shape of colloidal NPs [220]. The conventional electrodynamic theory confirmed that only ellipsoidal-shaped particles have homogenous magnetization and any distorting of the shape will lead to inhomogeneous magnetization [27b]. The shape of MNPs strongly affects their magnetization. For example, cubic MNPs have concentrated spins at the corners of cubic like a flower state [27b]. This will lead to water molecules association and relaxation locally around the cubic particles. This significantly induces r_2 values enhancement in cubic MNPs compared to spherical ones [27b]. Hyeon *et al.* [221] prepared cubic IONPs with a critical edge length of 22 nm and a greatly high r_2 value of 761 $m.M^{-1}.s^{-1}$. Phospholipid polyethylene glycols coated cubic IONPs can be used as high sensitive MRI contrast agent in pancreatic islets [222].

The octapod IONPs also showed extremely high r_2 value of ~ 761 $m.M^{-1}.s^{-1}$ [197] presented great potential ability as an MRI contrast agent of liver tumors in small mice. Other studies showed that hallow shaped manganese oxide NPs have higher both T_1 and T_2 relaxivities compared to water-soluble manganese oxide NPs that make them attractive as MRI contrast agents [223]. These results strongly confirm that shape modification of MNPs is one of the best ways to prepare MNPs for MRI contrast agents.

4.1.2. Magnetic particle imaging—Magnetic particle imaging (MPI) is an emerging tomographic technique with the ability to take high-resolution, excellent sensitivity, and real-time images from targeted tissues which lead to diagnosic imaging and guided therapy [224]. This technique uses the non-linear magnetization of MNPs tracer to generate maps of tracer distribution [225]. Over the past decade, MPI has been developed for cell tracking, cancerous tissue imaging, and angiography [226]. Even though MPI scanners are in the clinical trial stage, the efforts toward the development of MPI tracers for human imaging are ongoing. Because MPI relies heavily on tracer quality, its future success depends on MNPs development. Thanks to having no background signal from tissue and using low-frequency

magnetic fields, MPI exhibits excellent imaging contrast and has no effective depth attenuation.

The contrast imaging of MPI is strongly dependent on the characteristics of iron-based tracers. Superparamagnetic iron oxides (SPIOs) were first developed as MRI contrast agents. Because of the safety and biodegradability of SPIOs, they were gradually employed as MPI tracers [227]. SPIONs have a long retention time in the human body from hours to days. In PET and SPECT, employed tracers have shorter retention time, so high-energy probes are required in PET [228]. There are numerous MPI tracers that have either been approved by the Food and Drug Administration (FDA) or are in clinical trial phases [229]. Most approved MRI contrast agents can be used as MPI tracers. Ferucarbotran (Resovist) and ferumoxytol had been historically used as clinically-approved contrast agents for MRI of liver/spleen [230]. In recent years, synthesis, development, and optimization of MPI tracers have drawn significant scientific interest.

The image resolution in the MPI technique is strongly affected by particle core size and size distribution of employed tracers. It has been reported that using SPIOs with 25–30 nm in diameter has the best performance in MPI quality and resolution [231]. It is important to note that the development of MPI tracers needs further consideration for circulation time, cellular uptake, distribution, biocompatibility [232], crystal structure [233], and surface quality [234].

4.1.3. Multimodal imaging—A single imaging modality is usually incapable of providing detailed results about a tissue. CT-MRI images are used to give us detailed information about specific tissue [184]. Both accurate and sensitive images can be obtained by a combination of different medical imaging techniques such as MRI, CT, PET, and optical fluorescence [235]. Multifunctional NPs should be used for giving detailed information from different imaging modalities [236]. In the next sections, the advantages of using multimodal imaging such as T_1-T_2 MR imaging, CT-MR imaging, and MRI-PET/SPECT dual-modal imaging are explained.

4.1.3.1. T_1–T_2 dual-mode MRI contrast agents: T_1 and T_2 contrast agents can generate bright and dark signals. However, there are several endogenous artifacts that can strongly affect the sensitivity and accuracy of MR images, namely fat, hemorrhages, blood clots, and air [237]. High-quality MR images can be achieved by minimizing the effects of these endogenous artifacts.

Complementary T_1-weighted and T_2-weighted MR images can be used to dominate ambiguities with obtained MR images from diseased lesions. However, this requires the use of both T_1-weighted and T_2-weighted MRI agents (Figure 12a). T_1-weighted MRI signal (positive signal) and T_2-weighted MRI signal (negative signal) are available simultaneously by using dual-mode NP contrast agents (DMCA). There are different ways to make these DMCAs such as labeling T_1 signal agents on the surface of NPs, embedding T_1 contrast agents inside MNPs, and magnetically decoupled T_1 and T_2 contrast agents [238].

In order to increase contrast and clarification, direct and simple conjugation of T_1-weighted MRI contrast agents on the surface of T_2-weighted MRI agents is the simplest way to

develop a T_1-T_2 dual-mode MRI agent. Bae *et al.* [239] developed gadolinium-labeled magnetite nanoparticles (GMNPs) as T_1-T_2 dual-mode MRI agents (Figure 12b). In the synthesized GMNP structure, gadolinium acts as a T_1-weighted and magnetite acts as a T_2-weighted MRI contrast agent. The TEM image of the synthesized GMNPs shows a spherical morphology with high dispersion in deionized water (Figure 12c). The magnetic properties and crystal structure of the MNPs are not considerably altered after labeling with gadolinium. *In vivo* MRI experiments have been carried out to show the capability of a synthesized nano-system to act as a T_1-T_2 dual-mode MRI agent. Three types of MNPs were inserted into dorsal flanks of nude mice: 1) Magnevist (gadopentetate dimeglumine, a commercial T_1-weighted MRI contrast agent containing gadolinium oxide), 2) Feridex (Ferumoxides suspension, a commercial T_2-weighted MRI contrast agent containing iron oxide), and 3) synthesized GMNPs as a compound containing gadolinium and iron oxide and T_1-T_2 dual-mode MRI agent. Figure 12d shows that the injection of Magnevist increases the bright area in T_1-weighted MR images. Dark signals in T_2–weighted MR images are enhanced by injection of Feridex (Figure 12e). In addition, Figure 12f and g show that the bright signal increases and the signal drops significantly at the injection site of GMNPs on T_1- and T_2-weighted MR images, respectively. The r_1 of synthesized GMNPs was measured to be 11.17 $mM^{-1}s^{-1}$, which is significantly higher than the r_1 value for Magnevist (5.39 mM-1s-1). It can be concluded that synthesized NPs show the promising ability for dual T_1- and T_2-weighted MRI.

Another method to make T_1-T_2 dual-mode MRI agents is embedding T_1 paramagnetic agents into T_2 MNPs (Figure 13a). The magnetic strength of both T_1 and T_2 contrast agents increases at the same time by embedding the T_1 contrast agent inside the T_2 contrast material. Zhou *et al.* [42] embedded Gd_2O_3 (as T_1 contrast agent) inside the IONPs to develop a T_1-T_2 dual-mode MRI agent. TEM images of synthesized GdIO particles showed a monodisperse dispersion of 14 nm diameter NPs (Figure 13b). Their results also revealed that the magnetic strength of synthesized GdIO NPs is much weaker than MNPs with a similar size. *In vivo* experiments were performed by intravenous injection of synthesized GdIO NPs into BALB/c mice with a dose of 2 mg Fe/kg mouse for studying the performance of NPs as T_1-T_2 dual-mode MRI contrast agents. These contrast agents generated significantly brighter signals at T_1-weighted and darker signals at T_2-weighted MR images for a mouse liver (Figure 13c and d). The *in vivo* experiment was followed by injection of GdIO NPs into nude mice. Then, HepG2 liver cancer cells (with a dose of 2 mg Fe/kg mouse) were orthotopically inoculated (Figure 13e and f). The ratio of tumor-to-liver contrast is greatly increased to approximately 83 and 137% in the case of T_1-weighted and T_2-weighted MR images, respectively.

4.1.3.2. CT/MRI dual contrast agents: MRI is one of the best imaging techniques with unique abilities in providing high-resolution images especially from soft tissues [240]. CT provides geometrically accurate scans and gives high-quality images from hard tissues such as bone and less valuable information about the soft tissues, compared with MRI. Although MRI gives precious details about special defects and their effect on adjacent structures, both MRI and CT may be used to determine the best location for doing biopsy [241] and to provide in-depth information about some tumors such as pituitary and brain tumors [242]. CT

imaging is based on how different tissues attenuate X-rays. Elements with high atomic numbers−such as gold, iodine, tantalum, and lanthanides are preferred to improve contrast [243]. Because MR images are generally more sensitive than that of CT images, the total amount and concentration of CT contrast agents should be higher than the amount of MRI contrast agents in the final CT/MRI contrast agent compound [244].

4.1.3.3. MRI-PET/SPECT dual contrast agents: The nuclear imaging techniques for diagnosis are generated from gamma-rays emitted from decaying radioisotopes: ^{68}Ga, ^{124}I, ^{64}Cu, and ^{18}F for PET applications and ^{111}In and ^{131}I for SPECT applications. Despite these methods providing high image sensitivity images, they are limited by relatively poor spatial resolution [245]. The combination of MRI and PET or SPECT methods allows for obtaining highly sensitive, high quality, and accurate information for a specific tissue [246].

Arsenic (As) is one the most attractive radioisotope elements employed in PET applications because it has four positron-emitting ($^{70/71/72/74}$As) and three electron-emitting ($^{74/76/77}$As) components with a suitable half-life (52.6 min to 17.8 days). Chen *et al.* [247] labeled superparamagnetic iron oxide (as an MRI contrast agent) with As (as PET contrast agent) (*As-SPION) by mixing water-soluble SPIONs with *As^{III} or *As^{V} species (Figure 14a). The *in vivo* experiments were carried out by injection of two different NPs into BALB/c mice: *As NPs, a control sample, and modified PEG-coated SPIONs (*As-SPION@PEG) NPs. The PET images depict fast renal clearance and almost no liver uptake of *As (Figure 14b), while there is a strong radioactive signal from the liver (Figure 14c and d) in the case of *As-SPION@ PEG (or *As-SPIONs). MRI showed darker images from the liver and no notable change of signal from the kidney (or bladder) after the injection of synthesized NPs (Figure 14e).

Advances in imaging techniques will continue developing, but MNPs tools that will lead to several advancements of their own. Among imaging techniques, MRI has been considered as a high-contrast method to image tissues and organs without side effects. The combination of MRI with other imaging methods like CT, PET, and SPECT offers excellent detailed images from cancer tissue. Overall, iron oxide, gold, and As NPs have been extensively used in recent research as contrast agents of MRI, CT, and PET imaging methods, respectively. High valuable information from target tissue can be obtained by a combination of various medical imaging techniques such as MRI, CT, PET, and optical fluorescence using multiple contrast agents. In this way, GMNPs, iron oxide/gold hybrid NPs, as labeled iron oxide NPs are extensively used as T_1-T_2 dual-mode MRI, MRI/CT, and MRI-PET/SPECT contrast agents, respectively.

4.2. Biosensors

Early detection, diagnosis, and staging of cancer can significantly improve human life and impact clinical practice. Obtaining useful information about the early stages of cancer growth can help in the prevention of its growth and metastasis [234]. The tuning ability of MNPs makes them a suitable candidate for diagnostic tools with better sensitivity, easier operation, and systemic sampling. For example, MNPs can remain within the circulatory system and can interact with and collect protein samples of various tissues [248]. The MNPs

can later be localized by applying magnetic fields and even retracted for further analysis [249]. MNPs can also be used *in vitro* for continuous monitoring of cell cultures without the need to have a continuous flow system. MNPs can increase the signal strength of absorbed proteins to promote more accurate measurements in turbid samples (such as blood or urine) with no preparation [26].

Several techniques are being employed to detect biomarkers and cells using MNPs: superconducting quantum interference devices (SQUIDs) [250], magnetoresistive sensors [251], and Hall sensors [252]. These techniques are based on measuring the magnetic field emitted from magnetically-labeled biological targets. In conventional detection methods by magnetometers, MNP-labeled targets should be close to the sensing elements. Diagnostic magnetic resonance (DMR) uses NMR. In NMR magnetic fields, MNPs produce local magnetic fields that can affect the relaxation rate of surrounding water molecules [49]. DMR detection via NMR detectors has a high sensitivity for fast and multiplexed detection in the range of microliter sample volumes. Development of a multifunctional and sensitive DMR system can be employed in the detection of bacteria, identifying small numbers of cells, increasing the performance to analyze molecular levels in real time, and measurement of a series of protein biomarkers [253]. By using this technique, it is possible to detect nucleic acids at clinically relevant concentrations [254], bacteria [203], and tumor cells [255].

MNPs in the form of clusters have poor remnant magnetic moments without having an external magnetic field; remnant magnetic moments could be significantly enhanced in the presence of an external magnetic field [256]. If MNPs do not spontaneously aggregate under physiological body solutions, they do not have any superparamagnetic property. In addition, the ease of distribution of the MNPs and the possibility of immobilization of specific targeting reagents enable the detection of small size tumors at stages where the tumors are undetectable by many imaging modalities and the disease is asymptomatic.

NPs including a ceramic magnetic core surrounded by a biocompatible shell are the most common NPs used for detecting molecules. Aligned and local magnetic dipoles in aqueous solution ruin the coherency of spin-spin relaxation of water protons. This phenomenon affects the magnetic resonance signal that is evaluated by decreasing the T_1 and T_2 relaxation times. Since the transverse relaxivity of MNPs is higher than their longitudinal relaxivity, T_2 is more practical in biosensing applications [257]. The MNPs with higher r_2 relaxivity values are more capable to create tangible T_2 changes [258].

DMR assays use targeted MNPs to evaluate the spin-spin T_2 relaxation time of biological targets. Small biological specimens such as proteins and oligonucleotides are detected by magnetic relaxation switching (MRSw) effects [253]. MRSw is based on changes in the spatial state of MNPs in solution. By aggregating MNPs in solution, the r_2 changes and affects the corresponding T_2 value. An increase in the T_2 value occurs by reverse switching caused by enzymatic cleavage of preformed clusters.

The MNPs used in biosensors should show superparamagnetic characterizations, high stability in aqueous solutions to prevent their spontaneous aggregation, good surface chemistry to be easily modified for binding affinity molecules like peptides, and high

magnetization and transverse relaxivity [259]. It has been reported that Mn-, Co-, or Ni-doped ferrite NPs [203b, 260] and iron core MNPs [261] have suitable properties to use in the biosensors applications.

The MNPs employed in DMR applications should have the ability to improve DMR sensitivity. For this target, MNPs need to have high r_2 relaxivity. The r_2 relaxivity of MNPs has a direct relation with $M^2.d^2$ (M and d is magnetization strength and diameter of MNPs, respectively) [262]. MNPs with strong magnetization ability and a large magnetic core meet the requirements for having high r_2 relaxivity values. Additionally, it has been recommended that the hydrodynamic diameter of MNPs is less than 50 nm for biosensor applications in order to promote biological activity for binding to a cell surface [263]. Furthermore, small MNPs are more stable in physiological environments and have excellent superparamagnetic ability to prevent the spontaneous magnetic aggregation that occurs with larger MNPs [203b, 260].

Elemental NPs made of iron have higher chemical stability in aqueous body media, r_2 relaxivities, and magnetization strength than metal oxides [264]. Because of the high oxidation potential of the iron core, it should be protected by a coating that improves biocompatibility. To enhance the biocompatibility of iron, cross-linked iron oxide nanoparticles (CLIONPs) are generated as the main class of engineered compounds employed in DMR industries due to their chemical stability and biocompatibility [254]. Mostly, CLIONPs are composed of a SPION core (magnetite (Fe_3O_4) or maghemite (Fe_2O_3)) and biocompatible dextran coating.

MFe_2O_4 (M can be a ferromagnetic element such as Mn, Co, or Ni) has excellent magnetization strength and displays promising properties for use in biosensing applications. Among all the alloys, manganese doped ferrite (MnFe2O4) has excellent magnetic strength and high r_2 value [264]. Issadore *et al.* [265] developed a microfluidic biosensor system using $MnFe_2O_4$ NPs in order to detect cells at low concentrations (i.e. <100 cells per ml whole blood). Their findings show that using $MnFe_2O_4$ NPs in their developed biosensors are able to screen a large number of cells (i.e. on the order of 10^7 cells) in 1 min.

Lee *et al.* [11a] used manganese doped ferrite NPs with high transverse relaxivity, high magnetization strength, and suitable diameter (i.e. less than 16 nm) for the magnetic core. They used a small-molecule 2,3-dimercaptosuccinic acid for the coating in the NMR probe for improvement of signal-to-noise ratio (SNR). They targeted Mn-MNP to cancer cells by conjugating monoclonal antibodies (against HER2/neu, EGFR, or EpCAM) to the surface of the particle. The hydrodynamic diameter of synthesized particles was increased by attaching 10 antibody molecules per particle. The synthesized compound NPs had long-term stability under *in vivo* conditions. Detection sensitivity is evaluated by SNR of an NMR setup. The NMR probe has a solenoidal micro-coil embedded in a microfluidic structure to improve the SNR (Figure 15a). Modification of an old planar micro-coil system using a solenoidal coil resulted in a 350% improvement in NMR signal levels (Figure 15b). Lee *et al.* [11a] showed that their developed NMR system and high strength magnetic Mn-doped ferrite NPs result in improved detection sensitivity (Figure 15c). Using developed DMR system with $MnFe_2O_4$ NPs could improve detection systems to diagnose single-cell levels (~2 cells in 1μL

detection volume) (Figure 15d). These results confirm that this detection system is highly sensitive and capable to provide accurate biological diagnosis systems.

Obtaining valuable information about the early stages of cancer growth is of great importance in order to have improved cancer treatment outcomes. MNPs with critical size could potentially circulate in blood and gather important information from different tissues, especially cancerous or diseased environments. The DMR detection method using NMR is a fast way to provide high sensitivity for multiplexed detection in the range of microliter sample volumes. The MNPs with high r_2 relaxivity and dynamic diameter less than 50 nm are the best choice to use in DMR applications.

5. Combined cancer diagnosis and therapy

Synchronizing imaging and therapeutic agents is a great way of targeting disease sites without affecting healthy tissues. Employing MNPs applicable as both therapeutic and contrast agents may provide the advantages of imaging-guided therapy (IGT). IGT enables us to collect valuable information about the size and location of cancerous tissue before treatment and help clinicians evaluate the therapy efficiency during surgery [266]. Imaging modalities such as MRI, PET, SPECT, and CT are currently employed in IGT applications.

IGT can be employed through two different approaches: One is encapsulation or conjugation functional agents such as drugs and imaging contrast materials into a single NP. Another approach uses multifunctional agents that can act as imaging and therapeutic agents simultaneously [267]. All mentioned MNPs applicable as contrast agents in MRI, PET, CT, and SPECT can be potential multifunctional nanomaterials in the IGT approach.

One of the most commonly IGT approaches is the combination of the hyperthermia method with imaging techniques to augment treatment efficiency and avoid harm to normal tissues. This is because imaging modalities can show valuable information about a tumor site and distinguish it from surrounded normal tissues. Iron oxide NPs can be considered as the most commonly used agent in IGT. Some other NPs such as $Gd_{0.02}Fe_{2.98}O_4$ have been reported as modified iron oxide NPs with higher SAR value applicable in hyperthermia and MRI techniques [268].

6. Conclusions and future directions

MNPs show great potential in cancer diagnosis methods such as biosensors and imaging applications and later cancer treatments like hyperthermia and drug release methods. Size, chemical composition, shape, and assembly of MNPs can strongly affect their magnetization behavior and biomedical applications. Low biocompatibility, insufficient magnetic strength, low drug loading capacity, and difficulty in tuning their size for special biomedical applications limit clinical translation of MNPs. Surface modification of MNPs with the proper coating material and ligand has a great impact on cancer diagnosis and treatment capabilities.

Tuning MNP properties for the best performance in biomedical applications has been of great importance in recent years. The biocompatibility of MNPs is the main matter of

concern. One of the best ways for enhancing the biocompatibility of MNPs is functionalization with a generally safe coating. Inherent properties of the coating material and subsequent NP-cell interactions often determine the biocompatibility of MNPs.

Magnetic hyperthermia, heat generation in cancer tissue by MNPs such as Mn, Fe, Co, Ni, Zn, Gd, Mg, and their oxides, is one a promising way for cancer treatment. Using MNPs with high SAR value can generate a high amount of heat by using a lower magnetic field strength, which results in fewer side effects. IONPs have superparamagnetic properties in the particle sizes less than 12 nm.

One alternative way to overcome the limitations of chemotherapy is targeted drug delivery at the site of diseased tissue. Polymeric NPs and micelles, liposomes, carbon nanotubes, graphene oxide, MNPs, silica, and gold NPs with unique properties have been developed for overcoming barriers preventing effective delivery of drugs into the cancer tumors.

MNPs have an important role in increasing imaging resolution in methods such as MRI, PET, SPECT, CT, and multimodal imaging. Gd^{3+} compounds, Mn^{2+} compounds, and SPIONs are attractive agents to improve contrast and clarification.

Despite significant progress in the diagnosis and treatment of different kinds of cancers, there are several important challenges that prevent the proper treatment of cancer. Potentially, various MNPs can be differentiated in the body using imaging modalities to enable the quick phenotyping of cancer cells. Such analysis will facilitate the selection of anticancer drugs and better predict potential targets for metastasis. Another important area that can significantly increase patient life expectancy is the prevention of further metastasis. One potential solution is to utilize MNPs circulating in blood flow for capturing or binding to circulating tumor cells in order to direct the cancer cells to a planned region or an implanted device for their extraction. The affinity of modified MNPs to circulating tumor cells also enables localized delivery of anticancer drugs.

MNPs can be used as nanobiopsy systems for taking samples from remote tumors that are not easily accessible or located in critical places; such nanobiopsy systems can help with the design of treatment regimens to improve therapeutic outcomes. Another area that has recently drawn significant attention is cancer immunotherapy. Current strategies are based on the subcutaneous injection of vaccine carrying materials or the extraction of a patient’s cells in order to train the cells outside the body and reinjection of the trained cells. However, both strategies are challenging and can lead to complications. The use of MNPs for the delivery of vaccines and their ability for removal at any given timepoint make them an attractive tool for such treatments. Even though some applications of MNPs in cancer therapy such as hyperthermia treatment are controversial, MNPs are a strong clinical tool for reducing patient pain, enhancing their life expectancy, and increasing the success of cancer therapies.

Acknowledgements

The financial support from the National Institutes of Health (GM126831, AR073822), the University of Nebraska-Lincoln, and Nebraska Tobacco Settlement Biomedical Research Enhancement Funds are gratefully acknowledged.

References

[1]. a)Saghazadeh S, Rinoldi C, Schot M, Kashaf SS, Sharifi F, Jalilian E, Nuutila K, Giatsidis G, Mostafalu P, Derakhshandeh H, Adv. Drug Deliv.Rev. 2018, 127, 138; [PubMed: 29626550] b)Elkhoury K, Russell CS, Sanchez-Gonzalez L, Mostafavi A, Williams TJ, Kahn C, Peppas NA, Arab-Tehrany E, Tamayol A, Adv. Healthc. Mater. 2019, 8, 1900506.

[2]. a)Besenhard MO, Baber R, LaGrow AP, Mazzei L, Thanh NT, Gavriilidis A, Cryst. Eng. Comm. 2018, 20, 7082;b)Zhou X.-x., Liu J.-f., Jiang G.-b., Environ. Sci. Technol. 2017, 51, 3892. [PubMed: 28248108]

[3]. Farzin A, Ahmadian M, Fathi M, Mater. Sci. Eng. C 2013, 33, 2251.

[4]. Tong R, Langer R, Cancer J. 2015, 21, 314. [PubMed: 26222084]

[5]. Choi CHJ, Zuckerman JE, Webster P, Davis ME, Proc. Natl. Acad. Sci. 2011, 108, 6656. [PubMed: 21464325]

[6]. a)Yildirimer L, Thanh NT, Loizidou M, Seifalian AM, Nano today 2011, 6, 585; [PubMed: 23293661] b)ud Din F, Aman W, Ullah I, Qureshi OS, Mustapha O, Shafique S, Zeb A, Int. J. Nanomedicine 2017, 12, 7291. [PubMed: 29042776]

[7]. Alagiri M, Muthamizhchelvan C, Ponnusamy S, Synth. Met. 2011, 161, 1776.

[8]. Kallumadil M, Tada M, Nakagawa T, Abe M, Southern P, Pankhurst QA, J. Magn. Magn. Mater. 2009, 321, 3650.

[9]. a)Pankhurst QA, Connolly J, Jones SK, Dobson J, Phys J. D Appl. Phys. 2003, 36, R167;b)Dobson J, Drug Dev. Res. 2006, 67, 55.

[10]. Lee N, Hyeon T, Chem. Soc. Rev. 2012, 41, 2575. [PubMed: 22138852]

[11]. a)Lee H, Yoon T-J, Figueiredo J-L, Swirski FK, Weissleder R, Proc. Natl. Acad. Sci. 2009, 106, 12459; [PubMed: 19620715] b)Li G, Sun S, Wilson RJ, White RL, Pourmand N, Wang SX, Sens. Actuator A Phys. 2006, 126, 98.

[12]. Tran N, Webster TJ, J. Mater. Chem. 2010, 20, 8760.

[13]. Gupta AK, Gupta M, Biomaterials 2005, 26, 3995. [PubMed: 15626447]

[14]. Frullano L, Meade TJ, J. Biol. Inorg. Chem. 2007, 12, 939. [PubMed: 17659368]

[15]. Sivakumar Balasubramanian ARG, Nagaoka Y, Iwai S, Suzuki M, Kizhikkilot V, Yoshida Y, Maekawa T, Nair SD, Int. J. Nanomedicine 2014, 9, 437. [PubMed: 24531392]

[16]. Baronzio GF, Seta RD, D'Amico M, Baronzio A, Freitas I, Forzenigo G, Gramaglia A, Hager ED, in Hyperthermia in Cancer Treatment: A Primer, Springer 2006, p. 247.

[17]. Hegyi G, Szigeti GP, Szász A, Evid.-Based Complementary Altern. Med. 2013, 2013.

[18]. Mornet S, Vasseur S, Grasset F, Duguet E, J. Mater. Chem. 2004, 14, 2161.

[19]. a)Minev B, Cancer management in man: chemotherapy, biological therapy, hyperthermia and supporting measures, Springer Science & Business Media, 2011;b)Matsumine A, Kusuzaki K, Matsubara T, Shintani K, Satonaka H, Wakabayashi T, Miyazaki S, Morita K, Takegami K, Uchida A, Clin. Exp. Metastas. 2007, 24, 191.

[20]. a)Kantoff PW, Higano CS, Shore ND, Berger ER, Small EJ, Penson DF, Redfern CH, Ferrari AC, Dreicer R, Sims RB, N. Engl. J. Med. 2010, 363, 411; [PubMed: 20818862] b)Lee DW, Barrett DM, Mackall C, Orentas R, Grupp SA, AACR, 2012.

[21]. Kim J-E, Shin J-Y, Cho M-H, Arch. Toxicol. 2012, 86, 685. [PubMed: 22076106]

[22]. Neuberger T, Schöpf B, Hofmann H, Hofmann M, Von Rechenberg B, J. Magn. Magn. Mater. 2005, 293, 483.

[23]. Veiseh O, Sun C, Gunn J, Kohler N, Gabikian P, Lee D, Bhattarai N, Ellenbogen R, Sze R, Hallahan A, Nano Lett. 2005, 5, 1003. [PubMed: 15943433]

[24]. Sun C, Lee JS, Zhang M, Adv. Drug Deliv.Rev. 2008, 60, 1252. [PubMed: 18558452]

[25]. Redig AJ, McAllister SS, J. Intern. Med. 2013, 274, 113. [PubMed: 23844915]

[26]. Malekzad H, Zangabad PS, Mirshekari H, Karimi M, Hamblin MR, Nanotechnol. Rev. 2017, 6, 301. [PubMed: 29335674]

[27]. Zhang H, Liu XL, Zhang YF, Gao F, Li GL, He Y, Peng ML, Fan HM, Sci. China Life Sci. 2018, 61, 400; [PubMed: 29675551] b)Zhou Z, Yang L, Gao J, Chen X, Adv. Mater. 2019, 31, 1804567.

[28]. Jahangirian H, Kalantari K, Izadiyan Z, Rafiee-Moghaddam R, Shameli K, Webster TJ, Int. J. Nanomedicine 2019, 14, 1633. [PubMed: 30880970]

[29]. a)Antonyraj CA, Jeong J, Kim B, Shin S, Kim S, Lee K-Y, Cho JK, J. Ind. Eng. Chem. 2013, 19, 1056;b)Neville F, Pchelintsev NA, Broderick MJ, Gibson T, Millner PA, Nanotechnology 2009, 20, 055612;c)Staniland SS, Nanotechnologies for the Life Sciences: Online 2007.

[30]. Yazdani F, Seddigh M, Mater. Chem. Phys. 2016, 184, 318.

[31]. Malik MA, Wani MY, Hashim MA, Arab. J. Chem. 2012, 5, 397.

[32]. Park J, Lee E, Hwang NM, Kang M, Kim SC, Hwang Y, Park JG, Noh HJ, Kim JY, Park JH, Angew. Chem. Int. Ed. 2005, 44, 2872.

[33]. N. Kandpal, N. Sah, R. Loshali, R. Joshi, J. Prasad, 2014.

[34]. a)Wu S, Sun A, Zhai F, Wang J, Xu W, Zhang Q, Volinsky AA, Mater. Lett. 2011, 65, 1882;b)ElBayoumi TA, Torchilin VP, Liposomes: methods and protocols, volume 1: pharmaceutical nanocarriers, Humana Press, 2010.

[35]. Mohapatra S, Misra M, Mahajan V, Raja K, J. Catal. 2007, 246, 362.

[36]. Hasany S, Ahmed I, Rajan J, Rehman A, Nanosci. Nanotechnol. 2012, 2, 148.

[37]. Taratula O, Dani RK, Schumann C, Xu H, Wang A, Song H, Dhagat P, Taratula O, Int. J. Pharm. 2013, 458, 169. [PubMed: 24091153]

[38]. Fang C, Wang K, Stephen ZR, Mu Q, Kievit FM, Chiu DT, Press OW, Zhang M, ACS Appl. Mater. Interfaces. 2015, 7, 6674. [PubMed: 25751368]

[39]. Kim D-H, Vitol EA, Liu J, Balasubramanian S, Gosztola DJ, Cohen EE, Novosad V, Rozhkova EA, Langmuir 2013, 29, 7425. [PubMed: 23351096]

[40]. Hu SH, Liao BJ, Chiang CS, Chen PJ, Chen IW, Chen SY, Adv. Mater. 2012, 24, 3627. [PubMed: 22689346]

[41]. Zhou Z, Wang L, Chi X, Bao J, Yang L, Zhao W, Chen Z, Wang X, Chen X, Gao J, ACS nano 2013, 7, 3287. [PubMed: 23473444]

[42]. Zhou Z, Huang D, Bao J, Chen Q, Liu G, Chen Z, Chen X, Gao J, Adv. Mater. 2012, 24, 6223. [PubMed: 22972529]

[43]. Kievit FM, Stephen ZR, Wang K, Dayringer CJ, Sham JG, Ellenbogen RG, Silber JR, Zhang M, Mol. Oncol. 2015, 9, 1071. [PubMed: 25681012]

[44]. Kim D, Yu MK, Lee TS, Park JJ, Jeong YY, Jon S, Nanotechnology 2011, 22, 155101.

[45]. Bates D, Abraham S, Campbell M, Zehbe I, Curiel L, PLoS One 2014, 9, e97220.

[46]. Nafiujjaman M, Revuri V, Nurunnabi M, Cho KJ, Lee Y.-k., Chem. Comm. 2015, 51, 5687. [PubMed: 25715169]

[47]. a)Salimi M, Sarkar S, Saber R, Delavari H, Alizadeh AM, Mulder HT, Cancer Nanotechnol. 2018, 9, 7; [PubMed: 30363777] b)Adedoyin AA, Ekenseair AK, Nano Res. 2018, 11, 5049.

[48]. Kim Y-S, Lee TH, O'Neill BE, Biochem. Biophys. Res. Commun. 2015, 464, 51. [PubMed: 26032500]

[49]. Berthier C, Horvatić M, Julien M-H, Mayaffre H, Krämer S, C.R. Phys. 2017, 18, 331.

[50]. Holladay RT, Virginia Tech, 2016.

[51]. Rodriguez-Luccioni HL, Latorre-Esteves M, Méndez-Vega J, Soto O, Rodríguez AR, Rinaldi C, Torres-Lugo M, Int. J. Nanomedicine 2011, 6, 373. [PubMed: 21499427]

[52]. a)Franckena M, van der Zee J, Curr. Opin. Obstet. Gynecol. 2010, 22, 9; [PubMed: 20019611] b)Pennacchioli E, Fiore M, Gronchi A, Expert Rev. Anticancer Ther. 2009, 9, 199. [PubMed: 19192958]

[53]. Kobayashi T, Biotechnol. J. 2011, 6, 1342. [PubMed: 22069094]

[54]. Giustini AJ, Petryk AA, Cassim SM, Tate JA, Baker I, Hoopes PJ, Nano Life 2010, 1, 17.

[55]. Chatterjee DK, Diagaradjane P, Krishnan S, Ther. Deliv. 2011, 2, 1001. [PubMed: 22506095]

[56]. Kaur P, Aliru ML, Chadha AS, Asea A, Krishnan S, Int. J. Hyperthermia 2016, 32, 76. [PubMed: 26757879]

[57]. Shubitidze F, Kekalo K, Stigliano R, Baker I, J. Appl. Phys. 2015, 117, 094302.

[58]. Basel MT, Balivada S, Wang H, Shrestha TB, Seo GM, Pyle M, Abayaweera G, Dani R, Koper OB, Tamura M, Int. J. Nanomedicine 2012, 7, 297. [PubMed: 22287840]

[59]. Araya T, Kasahara K, Nishikawa S, Kimura H, Sone T, Nagae H, Ikehata Y, Nagano I, Fujimura M, Onco. Targets Ther. 2013, 6, 237. [PubMed: 23569387]

[60]. Chatterjee J, Bettge M, Haik Y, Chen CJ, J. Magn. Magn. Mater. 2005, 293, 303.

[61]. Thorat N, Patil R, Khot V, Salunkhe A, Prasad A, Barick K, Ningthoujam R, Pawar S, New J. Chem. 2013, 37, 2733.

[62]. Kolosnjaj-Tabi J, Di Corato R, Lartigue L, Marangon I, Guardia P, Silva AK, Luciani N, Clément O, Flaud P, Singh JV, ACS nano 2014, 8, 4268. [PubMed: 24738788]

[63]. Cherukuri P, Glazer ES, Curley SA, Adv. Drug Deliv. Rev. 2010, 62, 339. [PubMed: 19909777]

[64]. a)Shah RR, Dombrowsky AR, Paulson AL, Johnson MP, Nikles DE, Brazel CS, Mater. Sci. Eng. C 2016, 68, 18;b)Martinez-Boubeta C, Simeonidis K, Makridis A, Angelakeris M, Iglesias O, Guardia P, Cabot A, Yedra L, Estradé S, Peiró F, Sci. Rep. 2013, 3, 1652. [PubMed: 23576006]

[65]. Suto M, Hirota Y, Mamiya H, Fujita A, Kasuya R, Tohji K, Jeyadevan B, J. Magn. Magn. Mater. 2009, 321, 1493.

[66]. Jeyadevan B, J. Ceram. Soc. Jpn. 2010, 118, 391.

[67]. Ota S, Kitaguchi R, Takeda R, Yamada T, Takemura Y, Nanomaterials 2016, 6, 170.

[68]. Lévy M, Wilhelm C, Siaugue J-M, Horner O, Bacri J-C, Gazeau F, J. Phys-Condens. Mat. 2008, 20, 204133.

[69]. a)Zhai Y, Xie H, Gu H, Int. J. Hyperthermia 2009, 25, 65; [PubMed: 19219702] b)Ito A, Tanaka K, Honda H, Abe S, Yamaguchi H, Kobayashi T, J. Biosci. Bioeng. 2003, 96, 364. [PubMed: 16233538]

[70]. Huang HS, Hainfeld JF, Int. J. Nanomedicine 2013, 8, 2521. [PubMed: 23901270]

[71]. a)Kobayashi H, Watanabe R, Choyke PL, Theranostics 2014, 4, 81;b)Acharya S, Sahoo SK, Adv. Drug Deliv.Rev. 2011, 63, 170; [PubMed: 20965219] c)Maeda H, Wu J, Sawa T, Matsumura Y, Hori K, J. Control Release 2000, 65, 271; [PubMed: 10699287] d)Maeda H, Nakamura H, Fang J, Adv. Drug Deliv.Rev. 2013, 65, 71; [PubMed: 23088862] e)Iyer AK, Khaled G, Fang J, Maeda H, Drug Discov. Today 2006, 11, 812. [PubMed: 16935749]

[72]. Krishnan KM, IEEE Trans. Magn. 2010, 46, 2523. [PubMed: 20930943]

[73]. Saito S, Tsugeno M, Koto D, Mori Y, Yoshioka Y, Nohara S, Murase K, Int. J. Nanomedicine 2012, 7, 5415. [PubMed: 23091384]

[74]. Saptarshi SR, Duschl A, Lopata AL, J. Nanobiotechnology 2013, 11, 26. [PubMed: 23870291]

[75]. a)Grüttner C, Müller K, Teller J, Westphal F, Foreman A, Ivkov R, J. Magn. Magn. Mater. 2007, 311, 181;b)Liao S-H, Yang H-C, Horng H-E, Chieh J-J, Chen K, Chen H, Chen J, Liu C, Liu C, Wang L, Appl. Phys. Lett. 2013, 103, 243703.

[76]. a)Prantner AM, Nguyen CV, Scholler N, J. Biomed. Nanotechnol. 2013, 9, 1686; [PubMed: 24015498] b)Vigor KL, Kyrtatos PG, Minogue S, Al-Jamal KT, Kogelberg H, Tolner B, Kostarelos K, Begent RH, Pankhurst QA, Lythgoe MF, Biomaterials 2010, 31, 1307. [PubMed: 19889453]

[77]. a)Kumar M, Singh G, Arora V, Mewar S, Sharma U, Jagannathan N, Sapra S, Dinda AK, Kharbanda S, Singh H, Int. J. Nanomedicine 2012, 7, 3503; [PubMed: 22848174] b)Karmakar A, Xu Y, Mahmood MW, Zhang Y, Saeed LM, Mustafa T, Ali S, Biris AR, Biris AS, J. Mater. Chem. 2011, 21, 12761.

[78]. a)Jie L-Y, Cai L-L, Wang L-J, Ying X-Y, Yu R-S, Zhang M-M, Du Y-Z, Int. J. Nanomedicine 2012, 7, 3981; [PubMed: 22866005] b)Veiseh O, Kievit FM, Fang C, Mu N, Jana S, Leung MC, Mok H, Ellenbogen RG, Park JO, Zhang M, Biomaterials 2010, 31, 8032. [PubMed: 20673683]

[79]. Yu MK, Kim D, Lee IH, So JS, Jeong YY, Jon S, Small 2011, 7, 2241. [PubMed: 21648076]

[80]. Pala K, Serwotka A, Jeleń F, Jakimowicz P, Otlewski J, Int. J. Nanomedicine 2014, 9, 67.

[81]. Fortin-Ripoche J-P, Martina MS, Gazeau F, Ménager C, Wilhelm C, Bacri J-C, Lesieur S, Clément O, Radiology 2006, 239, 415. [PubMed: 16549622]

[82]. Dormer K, Awasthi V, Galbraith W, Kopke R, Chen K, Wassel R, J. Biomed. Nanotechnol. 2008, 4, 174.

[83]. Prasad K, Bazaka O, Chua M, Rochford M, Fedrick L, Spoor J, Symes R, Tieppo M, Collins C, Cao A, Materials 2017, 10, 884.

[84]. Acosta-Torres LS, López-Marín LM, Nunez-Anita RE, Hernández-Padrón G, Castaño VM, J. Nanomater. 2011, 2011, 12.

[85]. Dennis C, Jackson A, Borchers J, Ivkov R, Foreman A, Hoopes P, Strawbridge R, Pierce Z, Goerntiz E, Lau J, J. Phys. D Appl. Phys. 2008, 41, 134020.

[86]. Kawai N, Futakuchi M, Yoshida T, Ito A, Sato S, Naiki T, Honda H, Shirai T, Kohri K, Prostate 2008, 68, 784. [PubMed: 18302228]

[87]. Bae S, Lee SW, Takemura Y, Yamashita E, Kunisaki J, Zurn S, Kim CS, IEEE Trans. Magn. 2006, 42, 3566.

[88]. Kim D-H, Lee S-H, Kim K-N, Kim K-M, Shim I-B, Lee Y-K, J. Magn. Magn. Mater. 2005, 293, 320.

[89]. a)Wijaya A, Brown KA, Alper JD, Hamad-Schifferli K, J. Magn. Magn. Mater. 2007, 309, 15;b)Sharma R, Chen C, J. Nanopart. Res. 2009, 11, 671.

[90]. Nojima K, Ge S, Katayama Y, Ueno S, Iramina K, J. Appl. Phys. 2010, 107, 09B320.

[91]. Huber DL, Small 2005, 1, 482. [PubMed: 17193474]

[92]. Ondeck C, Habib A, Ohodnicki P, Miller K, Sawyer C, Chaudhary P, McHenry M, J. Appl. Phys. 2009, 105, 07B324.

[93]. Fantechi E, Campo G, Carta D, Corrias A, de Julián Fernández C, Gatteschi D, Innocenti C, Pineider F, Rugi F, Sangregorio C, J. Phys. Chem. C 2012, 116, 8261.

[94]. Gonzales-Weimuller M, Zeisberger M, Krishnan KM, J. Magn. Magn. Mater. 2009, 321, 1947. [PubMed: 26405373]

[95]. De la Presa P, Luengo Y, Multigner M, Costo R, Morales M, Rivero G, Hernando A, J. Phys. Chem. 2012, 116, 25602.

[96]. Song M, Zhang Y, Hu S, Song L, Dong J, Chen Z, Gu N, Colloid. Surf. A Physicochem. Eng. Asp. 2012, 408, 114.

[97]. Pradhan P, Giri J, Banerjee R, Bellare J, Bahadur D, J. Magn. Magn. Mater. 2007, 311, 282.

[98]. Liu XL, Fan HM, Yi JB, Yang Y, Choo ESG, Xue JM, Di Fan D, Ding J, J. Mater. Chem. 2012, 22, 8235.

[99]. Liu XL, Yang Y, Ng CT, Zhao LY, Zhang Y, Bay BH, Fan HM, Ding J, Adv. Mater. 2015, 27, 1939. [PubMed: 25655680]

[100]. Mehdaoui B, Meffre A, Lacroix L-M, Carrey J, Lachaize S, Gougeon M, Respaud M, Chaudret B, J. Magn. Magn. Mater. 2010, 322, L49.

[101]. Horev-Azaria L, Baldi G, Beno D, Bonacchi D, Golla-Schindler U, Kirkpatrick JC, Kolle S, Landsiedel R, Maimon O, Marche PN, Part. Fiber Toxicol. 2013, 10, 32.

[102]. Yang Y, Liu X, Lv Y, Herng TS, Xu X, Xia W, Zhang T, Fang J, Xiao W, Ding J, Adv. Funct. Mater. 2015, 25, 812.

[103]. Kim D-H, Rozhkova EA, Ulasov IV, Bader SD, Rajh T, Lesniak MS, Novosad V, Nat. Mater. 2010, 9, 165. [PubMed: 19946279]

[104]. Serantes D, Simeonidis K, Angelakeris M, Chubykalo-Fesenko O, Marciello M, Morales MDP, Baldomir D, Martinez-Boubeta C, J. Phys. Chem. 2014, 118, 5927.

[105]. Liu T-Y, Hu S-H, Liu D-M, Chen S-Y, Chen I-W, Nano Today 2009, 4, 52.

[106]. Lee J-H, Jang J.-t., Choi J.-s., Moon SH, Noh S.-h., Kim J.-w., Kim J-G, Kim I-S, Park KI, Cheon J, Nat. Nanotechnol. 2011, 6, 418. [PubMed: 21706024]

[107]. Percebom AM, Costa LHM, Adv. Colloid. Interfac. Sci. 2019.

[108]. Liu X, Peng ML, Li G, Miao YQ, Luo H, Jing G, He Y, Zhang C, Zhang F, Fan H, Nano Lett. 2019.

[109]. Behrouzkia Z, Joveini Z, Keshavarzi B, Eyvazzadeh N, Aghdam RZ, Oman Med. J. 2016, 31, 89. [PubMed: 27168918]

[110]. Zhang W, Wu C, Silva SRP, Taylor & Francis, 2018.

[111]. Brusentsova TN, Brusentsov NA, Kuznetsov VD, Nikiforov VN, J. Magn. Magn. Mater. 2005, 293, 298.

[112]. Giri J, Pradhan P, Sriharsha T, Bahadur D, J. Appl. Phys. 2005, 97, 10Q916.

[113]. Bagaria HG, Phillips JL, Nikles DE, Johnson DT, presented at AIChE Annual Meeting Conference Proceedings 2005.

[114]. Tran PH-L, Tran TT-D, Van Vo T, Lee B-J, Arch. Pharm. Res. 2012, 35, 2045. [PubMed: 23263800]

[115]. Kafrouni L, Savadogo O, Prog. Biomater. 2016, 5, 147. [PubMed: 27995583]

[116]. a)Horsman MR, Overgaard J, Clin. Oncol. 2007, 19, 418;b)Issels RD, Eur. J. Cancer 2008, 44, 2546. [PubMed: 18789678]

[117]. Storm FK, Kaiser LR, Goodnight JE, Harrison WH, Elliott RS, Gomes AS, Morton DL, Cancer 1982, 49, 1243. [PubMed: 7059946]

[118]. Masunaga S. i., Ono K, Takahashi A, Ohnishi K, Ohnishi T, Suzuki M, Nagata K, Kinashi Y, Nagasawa H, Uto Y, Cancer Sci. 2003, 94, 125. [PubMed: 12708486]

[119]. Oyama T, Kawamura M, Abiko T, Izumi Y, Watanabe M, Kumazawa E, Kuga H, Shiose Y, Kobayashi K, Oncol. Rep. 2007, 17, 653. [PubMed: 17273747]

[120]. Ohguri T, Imada H, Kato F, Yahara K, Morioka T, Nakano K, Korogi Y, Int. J. Hyperthermia 2006, 22, 1. [PubMed: 16423749]

[121]. Johannsen M, Thiesen B, Gneveckow U, Taymoorian K, Waldöfner N, Scholz R, Deger S, Jung K, Loening SA, Jordan A, Prostate 2006, 66, 97. [PubMed: 16114060]

[122]. Colombo R, Brausi M, Da Pozzo L, Salonia A, Montorsi F, Scattoni V, Roscigno M, Rigatti P, Eur. Urol. 2001, 39, 95. [PubMed: 11173946]

[123]. Borkamo ED, Schem B-C, Fluge Ø, Bruland O, Dahl O, Mella O, Int. J. Radiat. 2009, 75, 1562.

[124]. Gammon DC, Pillarisetty VG, Piperdi B, Dutton T, Zybert J, Wolfe SH, Nguyen E, Sbat D, Sullivan M, Whalen GF, Am. J. Health Syst. Pharm. 2009, 66, 1186. [PubMed: 19535657]

[125]. a)Diagaradjane P, Shetty A, Wang JC, Elliott AM, Schwartz J, Shentu S, Park HC, Deorukhkar A, Stafford RJ, Cho SH, Nano letters 2008, 8, 1492; [PubMed: 18412402] b)Liang Z, Li X, Xie Y, Liu S, Biomed. Mat. 2014, 9, 025012.

[126]. Spyratou E, Makropoulou M, Efstathopoulos EP, Georgakilas AG, Sihver L, Cancers 2017, 9, 173.

[127]. Chidambaram M, Manavalan R, Kathiresan K, J. Pharm. Pharm. Sci. 2011, 14, 67. [PubMed: 21501554]

[128]. a)Chandra A, Asian Journal of Pharmaceutics (AJP): Free full text articles from Asian J Pharm 2018, 12;b)Kumar G, Chaudhary KK, Misra K, Tripathi A, Int. J. Pharmacol. 2017, 13, 709.

[129]. Hillery AM, Lloyd AW, Swarbrick J, Drug delivery and targeting: for pharmacists and pharmaceutical scientists, Crc press, 2002.

[130]. Zhao Y, Vivero-Escoto JL, Slowing II, Trewyn BG, Lin VS, Expert Opin. Drug Deliv. 2010, 7, 1013. [PubMed: 20716017]

[131]. Pham X-H, Hahm E, Kim TH, Kim H-M, Lee SH, Lee Y-S, Jeong DH, Jun B-H, Sci. Rep. 2018, 8, 6290. [PubMed: 29674713]

[132]. Shim HE, Lee JY, Lee CH, Mushtaq S, Song HY, Song L, Choi S-J, Lee K, Jeon J, Chemosphere 2018, 207, 649. [PubMed: 29852464]

[133]. Lamb J, Holland JP, J. Nucl. Med. 2018, 59, 382. [PubMed: 29025988]

[134]. a)McDevitt MR, Sgouros G, Sofou S, Annu. Rev. Biomed. Eng. 2018, 20, 73; [PubMed: 29345977] b)Farzin L, Sheibani S, Moassesi ME, Shamsipur M, J. Biomed. Mater. Res. A 2019, 107, 251; [PubMed: 30358098] c)Chen F, Ehlerding EB, Cai W, J. Nucl. 2014, 55, 1919.

[135]. a)Kim D, Shin K, Kwon SG, Hyeon T, Adv. Mater. 2018, 30, 1802309;b)Gurunathan S, Kang M-H, Qasim M, Kim J-H, Int. J. Mol. Sci. 2018, 19, 3264.

[136]. Almohammadi A, Alqarni A, Alraddadi R, Alzahrani F, J. Cancer Educ. 2019, 1.

[137]. Gerber DE, Am. Fam. Physician 2008, 77.

[138]. Singh R, Lillard JW Jr, Exp. Mol. Pathol. 2009, 86, 215. [PubMed: 19186176]

[139]. Kohler N, Sun C, Fichtenholtz A, Gunn J, Fang C, Zhang M, Small 2006, 2, 785. [PubMed: 17193123]

[140]. Hua M-Y, Yang H-W, Chuang C-K, Tsai R-Y, Chen W-J, Chuang K-L, Chang Y-H, Chuang H-C, Pang S-T, Biomaterials 2010, 31, 7355. [PubMed: 20609471]

[141]. Palumbo MO, Kavan P, Miller W, Panasci L, Assouline S, Johnson N, Cohen V, Patenaude F, Pollak M, Jagoe RT, Front. Pharmacol. 2013, 4, 57. [PubMed: 23675348]

[142]. Brans B, Linden O, Giammarile F, Tennvall J, Punt C, Eur. J. Cancer 2006, 42, 994. [PubMed: 16564689]

[143]. Jeong JM, Chung J-K, Cancer Biother. Radio. 2003, 18, 707.

[144]. Heckl S, Curr. Med. Chem. 2007, 14, 1713. [PubMed: 17627509]

[145]. Ross JS, Fletcher JA, Bloom KJ, Linette GP, Stec J, Symmans WF, Pusztai L, Hortobagyi GN, Mol. Cell. Proteom. 2004, 3, 379.

[146]. Veiseh O, Gunn JW, Kievit FM, Sun C, Fang C, Lee JS, Zhang M, Small 2009, 5, 256. [PubMed: 19089837]

[147]. Verma A, Ann. Indian Acad. Neurol. 2018, 21, 3. [PubMed: 29720791]

[148]. Tomanin R, Scarpa M, Curr. Gene Ther. 2004, 4, 357. [PubMed: 15578987]

[149]. a)Kievit FM, Veiseh O, Bhattarai N, Fang C, Gunn JW, Lee D, Ellenbogen RG, Olson JM, Zhang M, Adv. Funct. Mater. 2009, 19, 2244; [PubMed: 20160995] b)Pan B, Cui D, Sheng Y, Ozkan C, Gao F, He R, Li Q, Xu P, Huang T, Cancer Res. 2007, 67, 8156. [PubMed: 17804728]

[150]. Medarova Z, Pham W, Farrar C, Petkova V, Moore A, Nat. Med. 2007, 13, 372. [PubMed: 17322898]

[151]. a)Bagherifard S, Tamayol A, Mostafalu P, Akbari M, Comotto M, Annabi N, Ghaderi M, Sonkusale S, Dokmeci MR, Khademhosseini A, Adv. Healthc. Mater. 2016, 5, 175; [PubMed: 26501166] b)Tamayol A, Hassani Najafabadi A, Mostafalu P, Yetisen AK, Commotto M, Aldhahri M, Abdel-wahab MS, Najafabadi ZI, Latifi S, Akbari M, Annabi N, Yun SH, Memic A, Dokmeci MR, Khademhosseini A, Sci. Rep. 2017, 7, 9220; [PubMed: 28835675] c)Saghazadeh S, Rinoldi C, Schot M, Kashaf SS, Sharifi F, Jalilian E, Nuutila K, Giatsidis G, Mostafalu P, Derakhshandeh H, Yue K, Swieszkowski W, Memic A, Tamayol A, Khademhosseini A, Adv. Drug Deliv.Rev. 2018, 127, 138. [PubMed: 29626550]

[152]. Sershen S, West J, Adv. Drug Deliv.Rev. 2002, 54, 1225. [PubMed: 12393303]

[153]. Mohamed MA, Fallahi A, El-Sokkary AMA, Salehi S, Akl MA, Jafari A, Tamayol A, Fenniri H, Khademhosseini A, Andreadis ST, Cheng C, Prog. Polym. Sci. 2019, 98, 101147.

[154]. Li Y, Huang G, Zhang X, Li B, Chen Y, Lu T, Lu TJ, Xu F, Adv. Funct. Mater. 2013, 23, 660.

[155]. Kost J, Wolfrum J, Langer R, J. Biomed. Mater. Res. 1987, 21, 1367. [PubMed: 3323204]

[156]. Gao F, Xie W, Miao Y, Wang D, Guo Z, Ghosal A, Li Y, Wei Y, Feng SS, Zhao L, Adv. Healthc. Mater. 2019, 1900203.

[157]. Ali A, Hira Zafar MZ, ul Haq I, Phull AR, Ali JS, Hussain A, Nanotechnol. Sci. Appl. 2016, 9, 49. [PubMed: 27578966]

[158]. Kumar SK, Jouault N, Benicewicz B, Neely T, Macromolecules 2013, 46, 3199.

[159]. a)Frade RF, Simeonov S, Rosatella AA, Siopa F, Afonso CA, Chemosphere 2013, 92, 100; [PubMed: 23561571] b)Marcu A, Pop S, Dumitrache F, Mocanu M, Niculite C, Gherghiceanu M, Lungu C, Fleaca C, Ianchis R, Barbut A, Appl. Surf. Sci. 2013, 281, 60.

[160]. Olusanya TO, Ahmad H, Rushdi R, Ibegbu DM, Smith JR, Elkordy AA, Molecules 2018, 23, 907.

[161]. Bozzuto G, Molinari A, Int. J. Nanomedicine 2015, 10, 975. [PubMed: 25678787]

[162]. Faria M, Cruz M, Gonçalves M, Carvalho A, Feio G, Martins M, Int. J. Pharm. 2013, 446, 183. [PubMed: 23422275]

[163]. Qiu D, An X, Chen Z, Ma X, Chem. Phys. Lipid. 2012, 165, 563.

[164]. Landon CD, Park J-Y, Needham D, Dewhirst MW, Open Nanomed. J, 2011, 3, 38. [PubMed: 23807899]

[165]. Roy D, Brooks WL, Sumerlin BS, Chem. Soc. Rev. 2013, 42, 7214. [PubMed: 23450220]

[166]. Stoychev G, Puretskiy N, Ionov L, Soft Matter. 2011, 7, 3277.

[167]. Qiu D, An X, Colloids Surf. B Biointerfaces 2013, 104, 326. [PubMed: 23290769]

[168]. Szymusiak M, Kalkowski J, Luo H, Donovan AJ, Zhang P, Liu C, Shang W, Irving T, Herrera-Alonso M, Liu Y, ACS Macro Lett. 2017, 6, 1005. [PubMed: 29308298]

[169]. Chen H, Li B, Qiu J, Li J, Jin J, Dai S, Ma Y, Gu Y, Nanoscale 2013, 5, 12409. [PubMed: 24165905]

[170]. a)Yang HY, Jang M-S, Li Y, Fu Y, Lee JH, Lee DS, J. Control Release 2019, 301, 157; [PubMed: 30905667] b)Yan L, Amirshaghaghi A, Huang D, Miller J, Stein JM, Busch TM, Cheng Z, Tsourkas A, Adv. Func. Mat. 2018, 28, 1707030;c)Yang HY, Fu Y, Li Y, Jang M-S, Lee JH, Lee DS, J. Mater. Chem. B 2018, 6, 5562. [PubMed: 32254966]

[171]. Saravanakumar G, Lee J, Kim J, Kim WJ, Chem. Comm. 2015, 51, 9995. [PubMed: 25998105]

[172]. Li Q, Li W, Di H, Luo L, Zhu C, Yang J, Yin X, Yin H, Gao J, Du Y, J. Control Release 2018, 277, 114. [PubMed: 29408424]

[173]. Hsu C-Y, Chen C-W, Yu H-P, Lin Y-F, Lai P-S, Biomaterials 2013, 34, 1204. [PubMed: 23069718]

[174]. a)Massoud TF, Gambhir SS, Genes Dev. 2003, 17, 545; [PubMed: 12629038] b)Hsu W, Markey MK, Wang MD, BMJ Publishing Group, 2013.

[175]. o. ES Radiology, Insights Imaging. 2011, 2, 621. [PubMed: 22347981]

[176]. Cruz LJ, Que I, Aswendt M, Chan A, Hoehn M, Löwik C, Nano Res. 2016, 9, 1276.

[177]. Antoch G, Bockisch A, Eur. J. Nucl. Med. Mol. Imaging. 2009, 36, 113.

[178]. Anderla A, Culibrk D, Delso G, Mirkovic M, Sci. World J. 2013, 2013.

[179]. Power SP, Moloney F, Twomey M, James K, O'Connor OJ, Maher MM, World J. Radiol. 2016, 8, 902. [PubMed: 28070242]

[180]. Milne S, King GG, J. Thorac. Dis. 2014, 6, 1570. [PubMed: 25478198]

[181]. Ono M, Wilson A, Nobrega J, Westaway D, Verhoeff P, Zhuang Z-P, Kung M-P, Kung HF, Nucl. Med. Biol. 2003, 30, 565. [PubMed: 12900282]

[182]. Spanoudaki VC, Ziegler SI, in Molecular Imaging I, Springer 2008, p. 53.

[183]. Bateman TM, J. Nucl. Cardiol. 2012, 19, 3.

[184]. Kircher MF, Willmann JK, Radiology 2012, 263, 633. [PubMed: 22623690]

[185]. Schenkman L, American Association for the Advancement of Science, 2011.

[186]. Mehrmohammadi M, Shin T-H, Qu M, Kruizinga P, Truby RL, Lee J-H, Cheon J, Emelianov SY, Nanoscale 2013, 5, 11179. [PubMed: 24080913]

[187]. Issa B, Obaidat IM, in Magnetic Resonance Imaging, IntechOpen 2019.

[188]. Plewes DB, Kucharczyk W, J. Magn. Reson. Imaging. 2012, 35, 1038. [PubMed: 22499279]

[189]. Tu C, Osborne EA, Louie AY, Ann. Biomed. Eng. 2011, 39, 1335. [PubMed: 21331662]

[190]. Mikawa M, Kato H, Okumura M, Narazaki M, Kanazawa Y, Miwa N, Shinohara H, Bioconjug. Chem. 2001, 12, 510. [PubMed: 11459454]

[191]. Ahmed HU, Kirkham A, Arya M, Illing R, Freeman A, Allen C, Emberton M, Nat. Rev. Clin. Oncol. 2009, 6, 197. [PubMed: 19333226]

[192]. Caravan P, Chem. Soc. Rev. 2006, 35, 512. [PubMed: 16729145]

[193]. Penfield JG, Reilly RF Jr, Nat. Rev. Nephrol. 2007, 3, 654.

[194]. a)Na HB, Lee JH, An K, Park YI, Park M, Lee IS, Nam DH, Kim ST, Kim SH, Kim SW, Angew. Chem. Int. Ed. 2007, 46, 5397;b)Taylor KM, Rieter WJ, Lin W, J. Am. Chem. Soc. 2008, 130, 14358; [PubMed: 18844356] c)Mertzman JE, Kar S, Lofland S, Fleming T, Van Keuren E, Tong YY, Stoll SL, Chem. Comm. 2009, 788.

[195]. Karki P, Lee E, Aschner M, Ann. Occup. Environ. Med. 2013, 25, 4. [PubMed: 24472696]

[196]. Markides H, Rotherham M, El Haj A, J. Nanomater. 2012, 2012, 13.

[197]. Zhao Z, Zhou Z, Bao J, Wang Z, Hu J, Chi X, Ni K, Wang R, Chen X, Chen Z, Nat. Commun. 2013, 4, 2266. [PubMed: 23903002]

[198]. Jun Y.-w., Huh Y-M, Choi J.-s., Lee J-H, Song H-T, Kim S, Kim S, Yoon S, Kim K-S, Shin J-S, J. Am. Chem. Soc. 2005, 127, 5732. [PubMed: 15839639]

[199]. Lu Y, Xu Y-J, Zhang G.-b., Ling D, Wang M.-q., Zhou Y, Wu Y-D, Wu T, Hackett MJ, Kim BH, Nat. Biomed. Eng. 2017, 1, 637. [PubMed: 31015599]

[200]. Kim BH, Lee N, Kim H, An K, Park YI, Choi Y, Shin K, Lee Y, Kwon SG, Na HB, J. Am. Chem. Soc. 2011, 133, 12624. [PubMed: 21744804]

[201]. Shah RR, Davis TP, Glover AL, Nikles DE, Brazel CS, J. Magn. Magn. Mater. 2015, 387, 96. [PubMed: 25960599]

[202]. O'handley RC, Modern magnetic materials: principles and applications, Wiley, 2000.

[203]. a)Joshi HM, Lin YP, Aslam M, Prasad P, Schultz-Sikma EA, Edelman R, Meade T, Dravid VP, J. Phys. Chem. 2009, 113, 17761;b)Lee J-H, Huh Y-M, Jun Y.-w., Seo J.-w., Jang J.-t., Song H-T, Kim S, Cho E-J, Yoon H-G, Suh J-S, Nat. Med. 2007, 13, 95. [PubMed: 17187073]

[204]. Wu M, Meng Q, Chen Y, Xu P, Zhang S, Li Y, Zhang L, Wang M, Yao H, Shi J, Adv. Funct. Mater. 2014, 24, 4273.

[205]. Wei H, Bruns OT, Kaul MG, Hansen EC, Barch M, Wiśniowska A, Chen O, Chen Y, Li N, Okada S, Proc. Natl. Acad. Sci. 2017, 114, 2325. [PubMed: 28193901]

[206]. Li Z, Wang SX, Sun Q, Zhao HL, Lei H, Lan MB, Cheng ZX, Wang XL, Dou SX, Lu GQ, Adv. Healthc. Mater. 2013, 2, 958. [PubMed: 23322490]

[207]. Chen R, Ling D, Zhao L, Wang S, Liu Y, Bai R, Baik S, Zhao Y, Chen C, Hyeon T, ACS nano 2015, 9, 12425. [PubMed: 26567968]

[208]. Yang L, Ma L, Xin J, Li A, Sun C, Wei R, Ren BW, Chen Z, Lin H, Gao J, Chem. Mater. 2017, 29, 3038.

[209]. Miao Y, Xie Q, Zhang H, Cai J, Liu X, Jiao J, Hu S, Ghosal A, Yang Y, Fan H, Theranostics 2019, 9, 1764. [PubMed: 31037137]

[210]. Wang Q, Shen M, Zhao T, Xu Y, Lin J, Duan Y, Gu H, Sci. Rep. 2015, 5, 7774. [PubMed: 25585607]

[211]. Tromsdorf UI, Bruns OT, Salmen SC, Beisiegel U, Weller H, Nano Lett. 2009, 9, 4434. [PubMed: 19799448]

[212]. Schwaminger S, Bauer D, Fraga-García P, Wagner F, Berensmeier S, Cryst. Eng. Comm. 2017, 19, 246.

[213]. Guo J, Yang W, Wang C, Adv. Mater. 2013, 25, 5196. [PubMed: 23996652]

[214]. Pöselt E, Kloust H, Tromsdorf U, Janschel M, Hahn C, Maßlo C, Weller H, Acs Nano 2012, 6, 1619. [PubMed: 22276942]

[215]. Yoon TJ, Lee H, Shao H, Hilderbrand SA, Weissleder R, Adv. Mater. 2011, 23, 4793. [PubMed: 21953810]

[216]. Abakumov MA, Nukolova NV, Sokolsky-Papkov M, Shein SA, Sandalova TO, Vishwasrao HM, Grinenko NF, Gubsky IL, Abakumov AM, Kabanov AV, Nanomed- Nanothechnol. 2015, 11, 825.

[217]. Covarrubias G, Cha A, Rahmy A, Lorkowski M, Perera V, Erokwu BO, Flask C, Peiris PM, Schiemann WP, Karathanasis E, PloS one 2018, 13, e0204296.

[218]. Davies G-L, Kramberger I, Davis JJ, Chem. Comm. 2013, 49, 9704. [PubMed: 24040650]

[219]. Stephen ZR, Kievit FM, Zhang M, Mater. Today 2011, 14, 330.

[220]. Jeong H-H, Mark AG, Alarcón-Correa M, Kim I, Oswald P, Lee T-C, Fischer P, Nat. Commun. 2016, 7, 11331. [PubMed: 27090866]

[221]. Lee N, Choi Y, Lee Y, Park M, Moon WK, Choi SH, Hyeon T, Nano Lett. 2012, 12, 3127. [PubMed: 22575047]

[222]. Lee N, Kim H, Choi SH, Park M, Kim D, Kim H-C, Choi Y, Lin S, Kim BH, Jung HS, Proc. Natl. Acad. Sci. 2011, 108, 2662. [PubMed: 21282616]

[223]. Shin J, Anisur RM, Ko MK, Im GH, Lee JH, Lee IS, Angew. Chem. Int. Ed. 2009, 48, 321.

[224]. Goodwill PW, Konkle JJ, Zheng B, Saritas EU, Conolly SM, IEEE Trans. Med. Imaging 2012, 31, 1076. [PubMed: 22552332]

[225]. Rahmer J, Antonelli A, Sfara C, Tiemann B, Gleich B, Magnani M, Weizenecker J, Borgert J, Phys. Med. Biol. 2013, 58, 3965. [PubMed: 23685712]

[226]. Wang Y-XJ, Quant. Imaging Med. Surg. 2011, 1, 35. [PubMed: 23256052]

[227]. Panagiotopoulos N, Duschka RL, Ahlborg M, Bringout G, Debbeler C, Graeser M, Kaethner C, Luedtke-Buzug K, Medimagh H, Stelzner J, Int. J. Nanomedicine 2015, 10, 3097. [PubMed: 25960650]

[228]. Bauer LM, Situ SF, Griswold MA, Samia ACS, J. Phys. Chem. Lett. 2015, 6, 2509. [PubMed: 26266727]

[229]. Reimer P, Balzer T, Eur. Radiol. 2003, 13, 1266. [PubMed: 12764641]

[230]. a)Ferguson RM, Minard KR, Khandhar AP, Krishnan KM, Med. Phys. 2011, 38, 1619; [PubMed: 21520874] b)Ferguson RM, Minard KR, Krishnan KM, J. Magn. Magn. Mater. 2009, 321, 1548. [PubMed: 19606261]

[231]. Wu L, Zhang Y, Steinberg G, Qu H, Huang S, Cheng M, Bliss T, Du F, Rao J, Song G, Am. J. Neuroradiol. 2019, 40, 206. [PubMed: 30655254]

[232]. Song G, Chen M, Zhang Y, Cui L, Qu H, Zheng X, Wintermark M, Liu Z, Rao J, Nano lett. 2017, 18, 182. [PubMed: 29232142]

[233]. Starmans LW, Moonen RP, Aussems-Custers E, Daemen MJ, Strijkers GJ, Nicolay K, Grüll H, PLOS one 2015, 10, e0119257.

[234]. Fass L, Mol. Oncol. 2008, 2, 115. [PubMed: 19383333]

[235]. Cho EC, Glaus C, Chen J, Welch MJ, Xia Y, Trends Mol. Med. 2010, 16, 561. [PubMed: 21074494]

[236]. Jun Y.-w., Seo J.-w., Cheon J, Acc. Chem. Res. 2008, 41, 179. [PubMed: 18281944]

[237]. Bulte JW, Kraitchman DL, NMR Biomed. 2004, 17, 484. [PubMed: 15526347]

[238]. Shin T-H, Choi J.-s., Yun S, Kim I-S, Song H-T, Kim Y, Park KI, Cheon J, ACS nano 2014, 8, 3393. [PubMed: 24673493]

[239]. Bae KH, Kim YB, Lee Y, Hwang J, Park H, Park TG, Bioconjug. Chem. 2010, 21, 505. [PubMed: 20166678]

[240]. Haffner-Luntzer M, Müller-Graf F, Matthys R, Hägele Y, Fischer V, Jonas R, Abaei A, Gebhard F, Rasche V, Ignatius A, PloS one 2017, 12, e0174283.

[241]. Taghipour Zahir S, Dehghani F, Iran. J. Pediatr. Hematol. Oncol. 2011, 1, 121.

[242]. a)Prabhakar R, Haresh K, Ganesh T, Joshi R, Julka P, Rath G, J. Cancer Res. Ther. 2007, 3, 121; [PubMed: 17998738] b)Taku N, Koulouri O, Scoffings D, Gurnell M, Burnet N, BJR| case reports 2017, 20160098.

[243]. Lusic H, Grinstaff MW, Chem. Rev. 2012, 113, 1641. [PubMed: 23210836]

[244]. Hagit A, Soenke B, Johannes B, Shlomo M, Biomacromolecules 2010, 11, 1600. [PubMed: 20443579]

[245]. Lee D-E, Koo H, Sun I-C, Ryu JH, Kim K, Kwon IC, Chem. Soc. Rev. 2012, 41, 2656. [PubMed: 22189429]

[246]. Choi J. s., Park JC, Nah H, Woo S, Oh J, Kim KM, Cheon GJ, Chang Y, Yoo J, Cheon J, Angew. Chem. Int. Ed. 2008, 47, 6259.

[247]. Chen F, Ellison PA, Lewis CM, Hong H, Zhang Y, Shi S, Hernandez R, Meyerand ME, Barnhart TE, Cai W, Angew. Chem. Int. Ed. 2013, 52, 13319.

[248]. Hasan A, Morshed M, Memic A, Hassan S, Webster TJ, Marei HE-S, Int. J. Nanomedicine 2018, 13, 5637. [PubMed: 30288038]

[249]. Gaster RS, Xu L, Han S-J, Wilson RJ, Hall DA, Osterfeld SJ, Yu H, Wang SX, Nat. Nanotechnol. 2011, 6, 314. [PubMed: 21478869]

[250]. Schaller V, Sanz-Velasco A, Kalabukhov A, Schneiderman JF, Öisjöen F, Jesorka A, Astalan AP, Krozer A, Rusu C, Enoksson P, Lab Chip. 2009, 9, 3433. [PubMed: 19904412]

[251]. Gaster RS, Hall DA, Nielsen CH, Osterfeld SJ, Yu H, Mach KE, Wilson RJ, Murmann B, Liao JC, Gambhir SS, Nat. Med. 2009, 15, 1327. [PubMed: 19820717]

[252]. Aytur T, Foley J, Anwar M, Boser B, Harris E, Beatty PR, J. Immunol. Methods 2006, 314, 21. [PubMed: 16842813]

[253]. Lee H, Sun E, Ham D, Weissleder R, Nat. Med. 2008, 14, 869. [PubMed: 18607350]

[254]. Perez JM, Josephson L, O'Loughlin T, Högemann D, Weissleder R, Nat. Biotechnol. 2002, 20, 816. [PubMed: 12134166]

[255]. a)Haun JB, Castro CM, Wang R, Peterson VM, Marinelli BS, Lee H, Weissleder R, Sci. Transl. Med. 2011, 3, 71ra16;b)Haun JB, Devaraj NK, Marinelli BS, Lee H, Weissleder R, ACS nano 2011, 5, 3204. [PubMed: 21351804]

[256]. Issa B, Obaidat IM, Albiss BA, Haik Y, Int. J. Mol. Sci. 2013, 14, 21266. [PubMed: 24232575]

[257]. Shao H, Min C, Issadore D, Liong M, Yoon T-J, Weissleder R, Lee H, Theranostics 2012, 2, 55. [PubMed: 22272219]

[258]. Mishra SK, Kumar BH, Khushu S, Tripathi RP, Gangenahalli G, Contrast Media Mol. Imaging 2016, 11, 350. [PubMed: 27230705]

[259]. Koh I, Josephson L, sensors 2009, 9, 8130. [PubMed: 22408498]

[260]. Jun YW, Lee JH, Cheon J, Angew. Chem. Int. Ed. 2008, 47, 5122.

[261]. a)Miguel OB, Gossuin Y, Morales M, Gillis P, Muller R, Veintemillas-Verdaguer S, Magn. Reson. Imaging 2007, 25, 1437; [PubMed: 17566686] b)Peng S, Wang C, Xie J, Sun S, J. Am. Chem. Soc. 2006, 128, 10676. [PubMed: 16910651]

[262]. Brooks RA, Moiny F, Gillis P, Magn. Reson. Med. 2001, 45, 1014. [PubMed: 11378879]

[263]. Chithrani BD, Chan WC, Nano Lett. 2007, 7, 1542. [PubMed: 17465586]

[264]. Tromsdorf UI, Bigall NC, Kaul MG, Bruns OT, Nikolic MS, Mollwitz B, Sperling RA, Reimer R, Hohenberg H, Parak WJ, Nano Lett. 2007, 7, 2422. [PubMed: 17658761]

[265]. Issadore D, Chung J, Shao H, Liong M, Ghazani AA, Castro CM, Weissleder R, Lee H, Sci. Transl. Med. 2012, 4, 141ra92.

[266]. Ju Y, Dong B, Yu J, Hou Y, Nano Today 2019.

[267]. Drake P, Cho H-J, Shih P-S, Kao C-H, Lee K-F, Kuo C-H, Lin X-Z, Lin Y-J, J. Mater. Chem. 2007, 17, 4914.

[268]. a)Gleich B, Weizenecker J, Borgert J, Phys. Med. Biol. 2008, 53, N81; [PubMed: 18367783] b)Konkle JJ, Goodwill PW, Carrasco-Zevallos OM, Conolly SM, IEEE Trans. Med. Imaging 2012, 32, 338. [PubMed: 23193308]

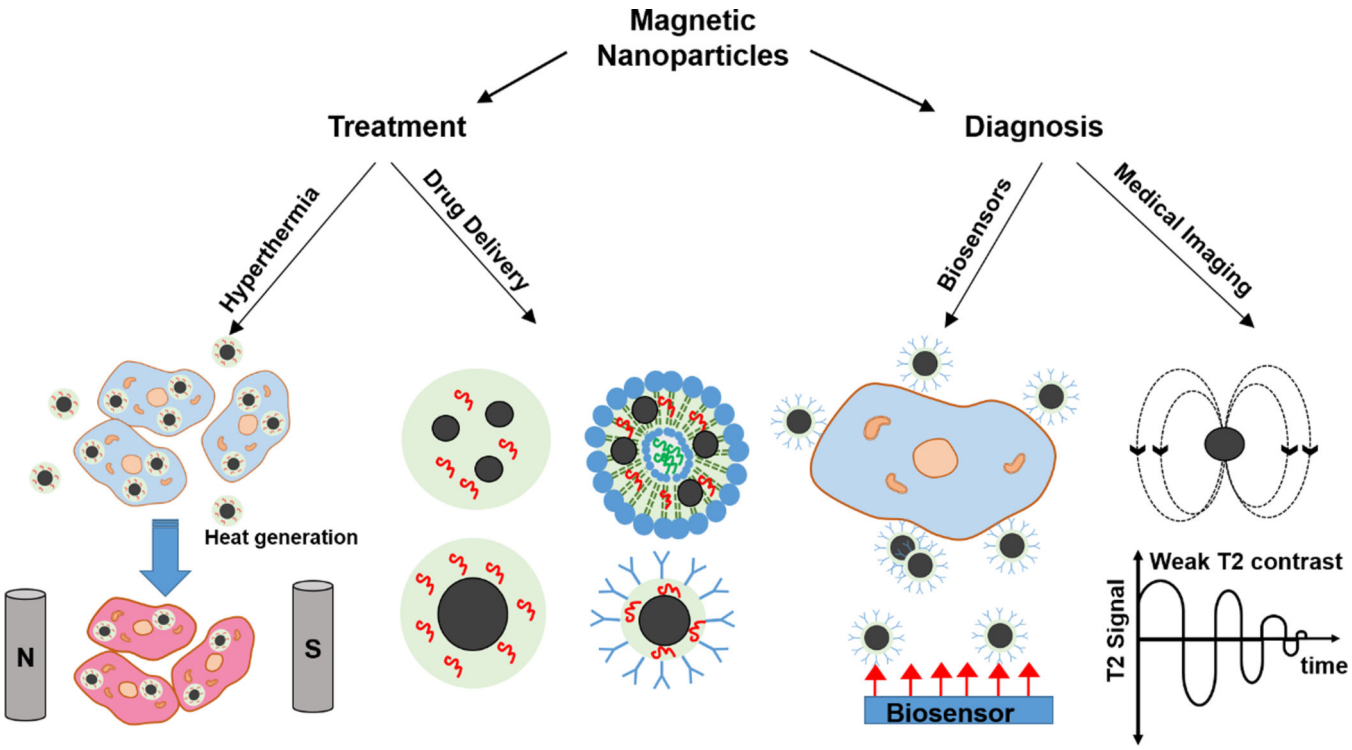

Figure 1.

Different forms of the MNPs with considerable potential in hyperthermia, drug delivery, imaging, and biosensing for cancer treatment and diagnosis.

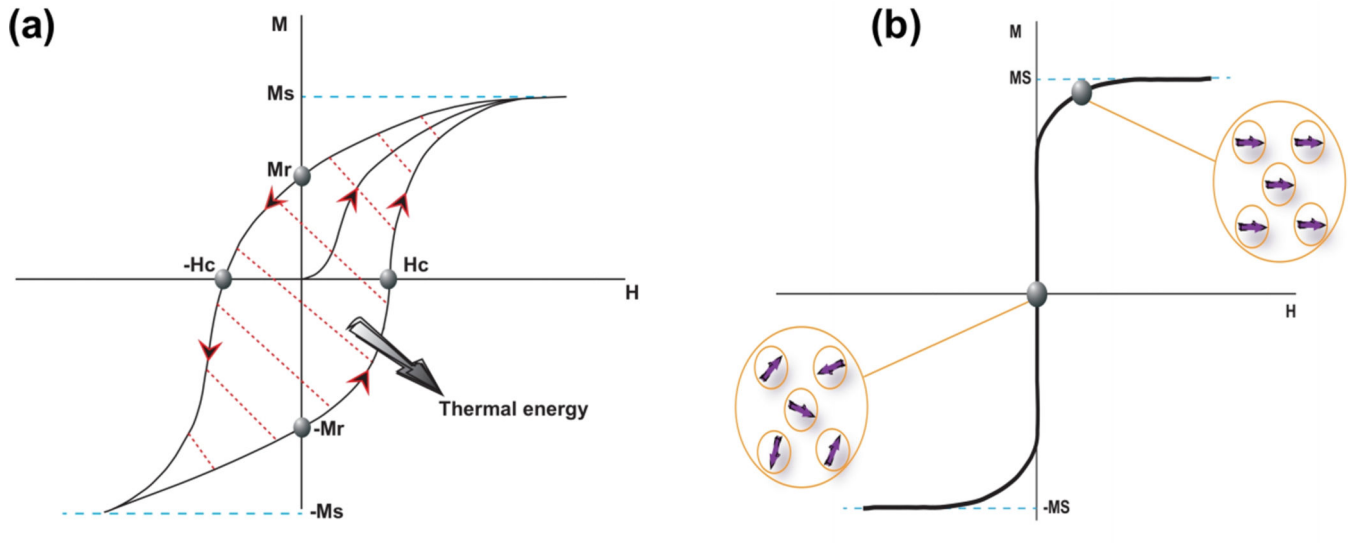

Figure 2.
Schematic drawing of (a) a hysteresis loop of a ferromagnetic material and (b) typical plot of a superparamagnetic material.

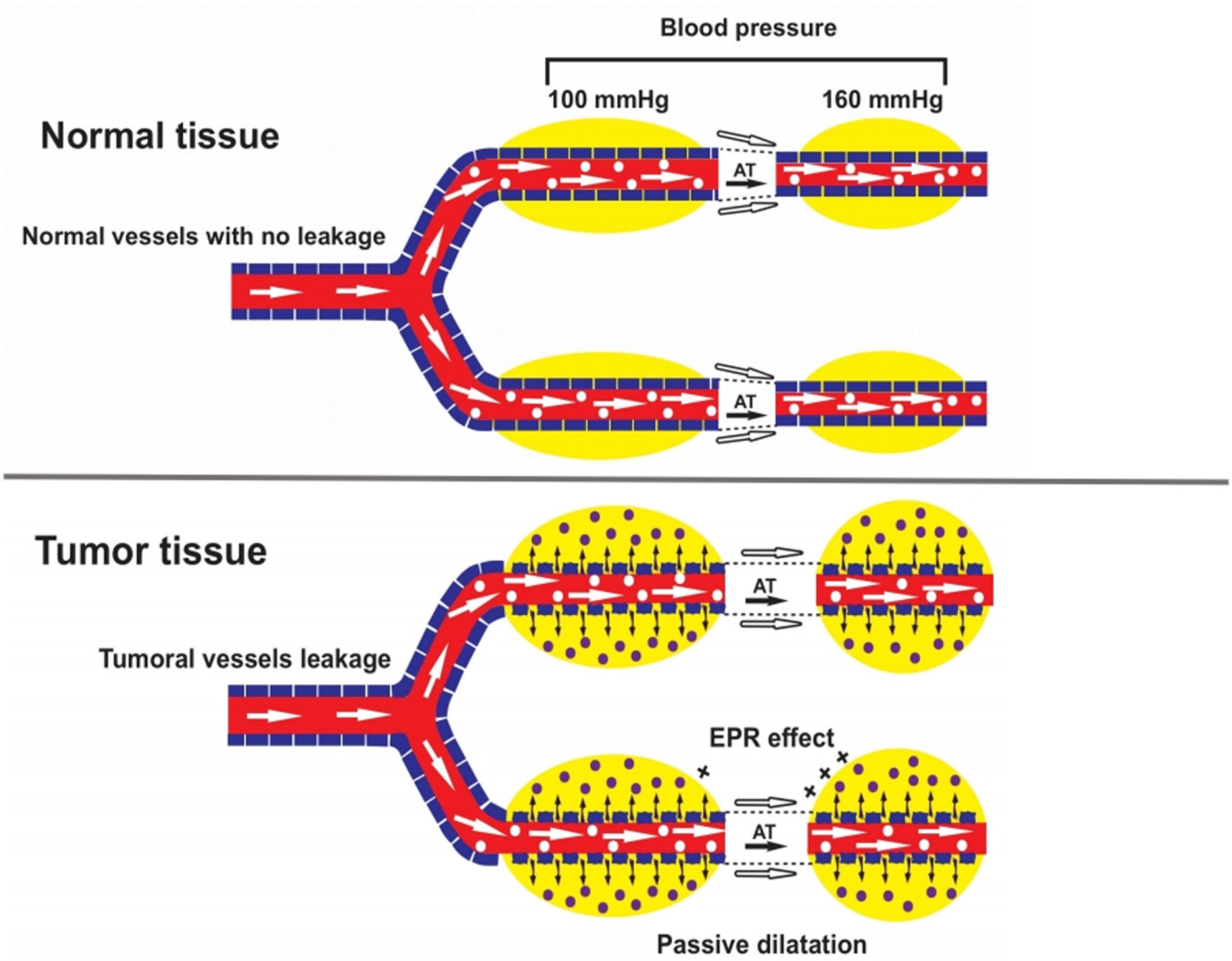

Figure 3:
Schematic representation of the EPR effect in normal and cancer tissue.

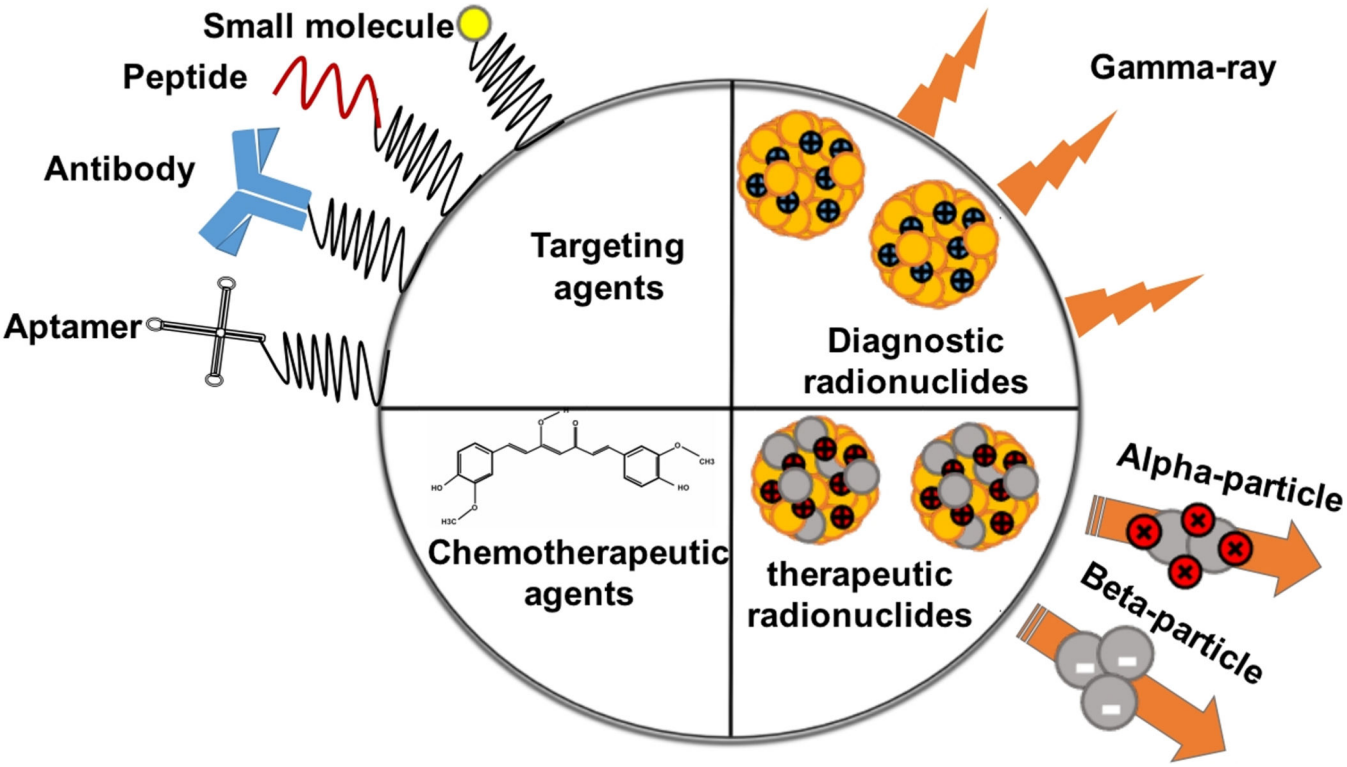

Figure 4:
Multifunctional MNPs in cancer therapy and diagnosis.

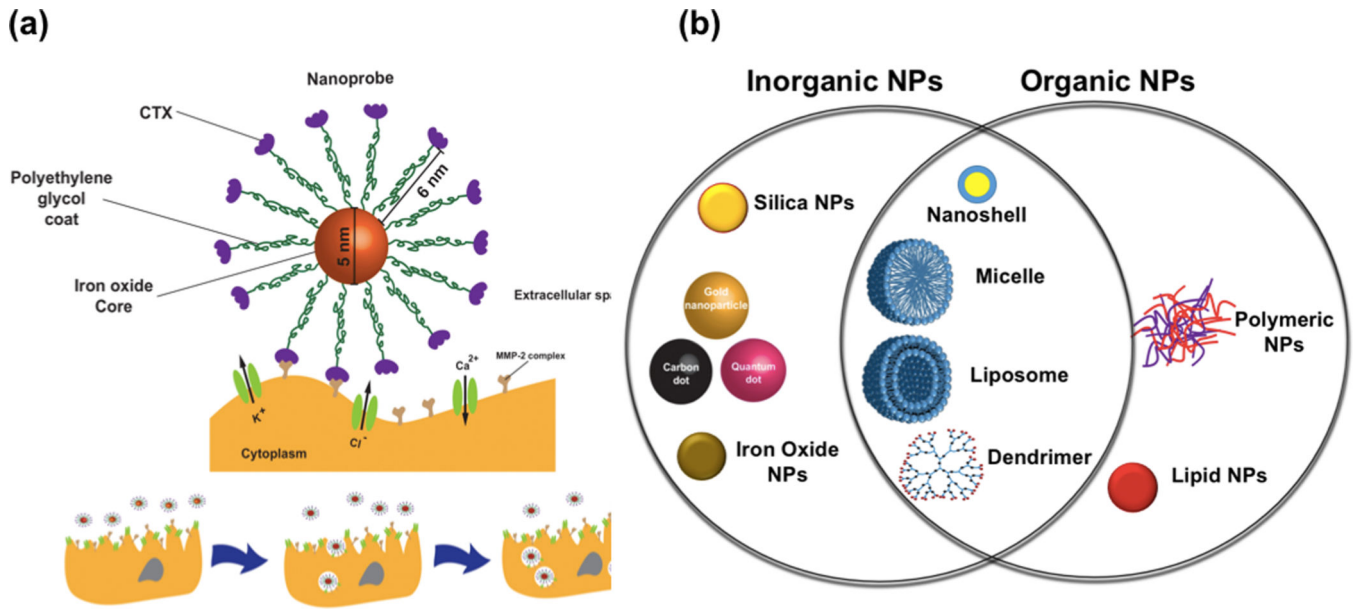

Figure 5.

(a) Schematic illustrations of NPC inhibiting tumor cell invasion. Different elements of NPC are stuck to the surface of glioma cells and the effect of NPCs on cell morphology; Reproduced with permission from Veiseh *et al.* [146] Copyright (2009) Wiley-VCH. (b) Schematic representation of different nano-systems for application in thermo-chemotherapy.

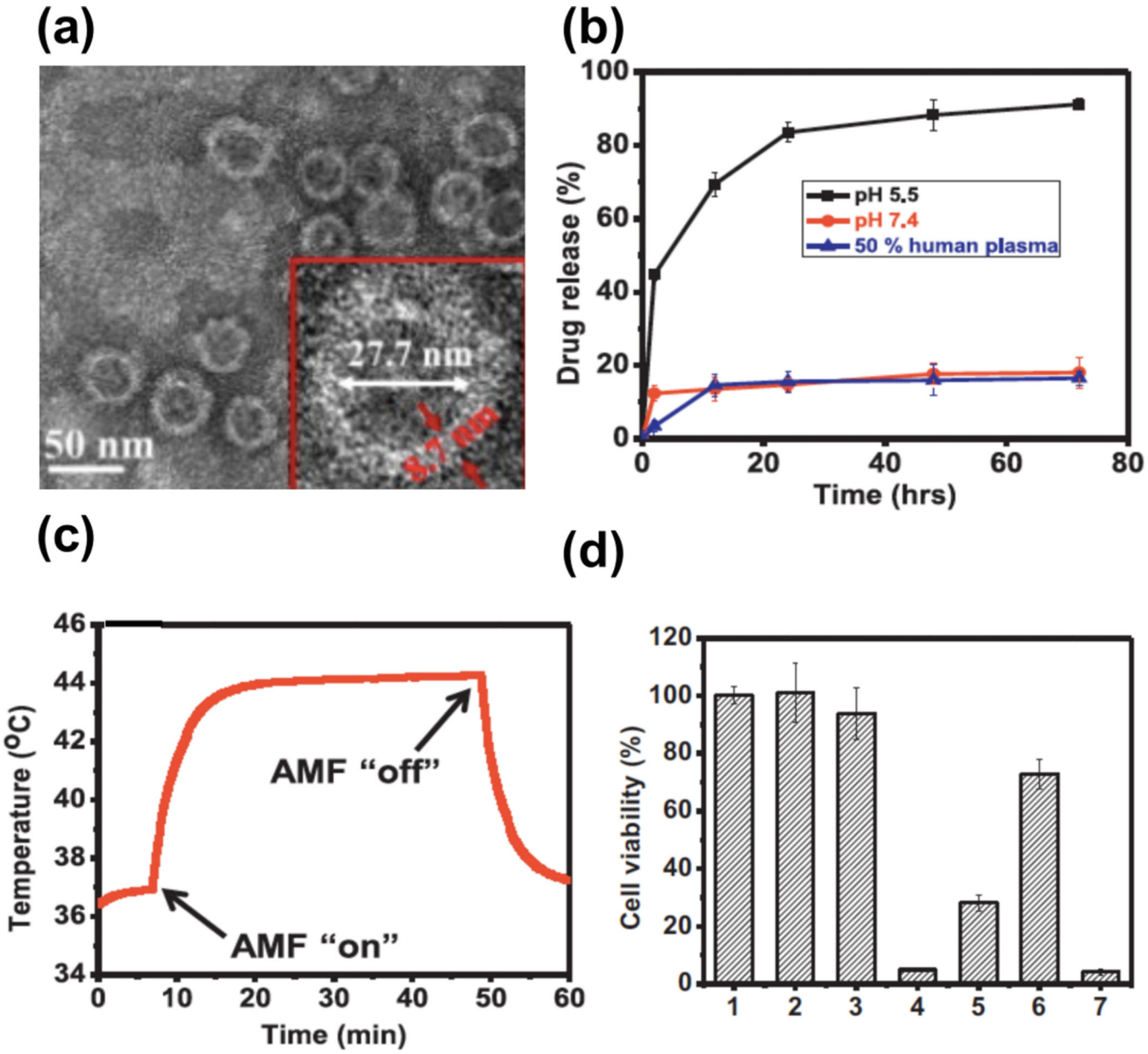

Figure 6.

(a) TEM image of DOX loaded NPs modified with PEG and LHRH peptide. (b) Release curve of DOX from iron oxide- DOX-PEG-LHRH nano-system incubated at 37˚C at different pH levels. (c) The dynamic temperature profile of the synthesized core/shell system under AMF (33.5 kA/m and 393 kHz). (d) Viability of A2780/AD ovarian cancer cells after curing with the following: (1) control (no treatment), (2) exposed only to AMF, (3) including only synthesized core/shell nano-system, (4) 44˚C hyperthermia for 30 min: incubation of cells with IONPs-PEG-LHRH nano-system and exposure to AMF (33.5 kA/m and398 kHz), (5) 40˚C hyperthermia for 30 min: incubation of cells with IONPs-PEG-LHRH nano-system and exposure to AMF (21.2 kA/m and 393 kHz), (6) chemotherapy: cells treatment with IONPS-DOX-PEG-LHRH, and (7) combinatorial treatment: chemotherapy and

hyperthermia (40˚C for 30 min). (a-d) Reprinted with permission from Taratula *et al.* [37] Copyright (2013) Elsevier.

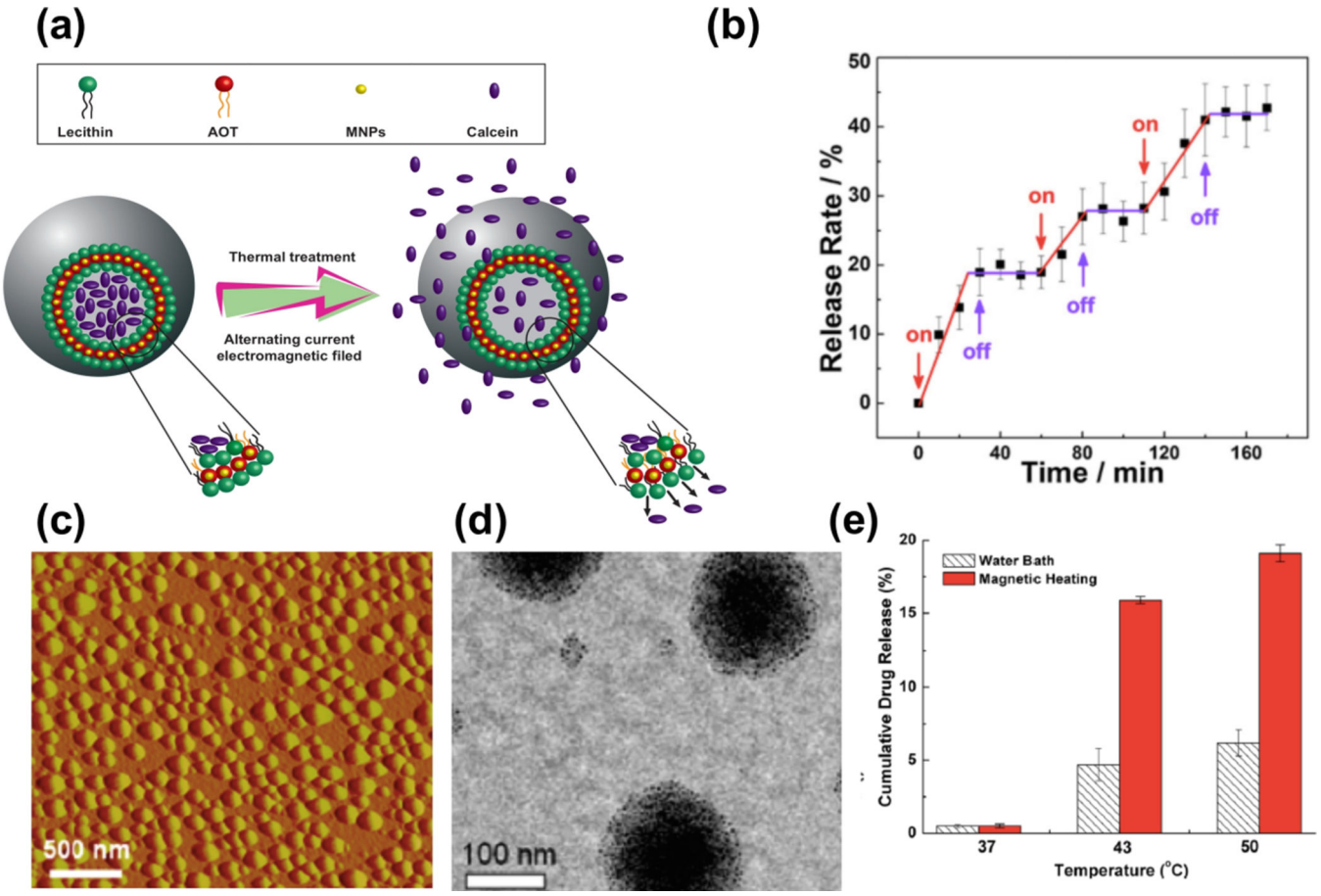

Figure 7.

(a) Schematic representation of drug release from liposomes with hydrophobic MNPs in lipid bilayer. (b) The release rate of calcein-loaded magnetoliposomes vs. time over three successive on/off cycles under external AMF at room temperature (Reprinted with permission from Qiu *et al.* [167] Copyright (2013) Elsevier). (c) Topographic atomic force microscope image from the loaded micelles with magnetic iron oxide. (d) A TEM image of synthesized micelles. (e) DOX cumulative drug release vs. temperature from synthesized micelles in a hot water bath and magnetically induced heating. (c-e) Reprinted with permission from Kim *et al.* [39] Copyright (2013) American Chemical Society.

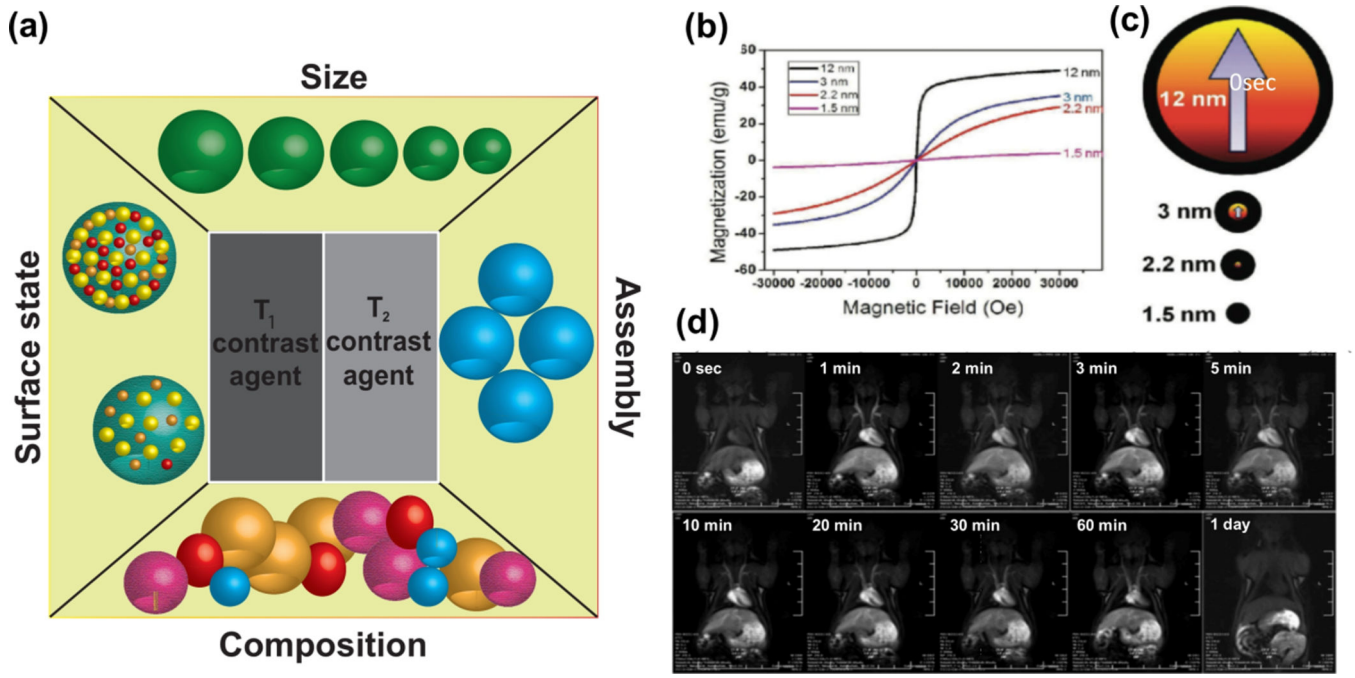

Figure 8.

(a) Various properties of MNPs affecting the r_2/r_1 ratio and consequently on MR image contrast. (b) Magnetization curve of magnetic IONPs of different diameters (1.5, 2.2, 3 and 12nm). (c) A schematic of the spin canting effect of different sizes of IONPs. Red and black colors correspond to the magnetic core and disorder shell, respectively. (d) MR images from a rat after injection of IONPs at various time periods. (b-d) Reprinted with permission from Kim *et al.* [200] Copyright (2011) American Chemical Society.

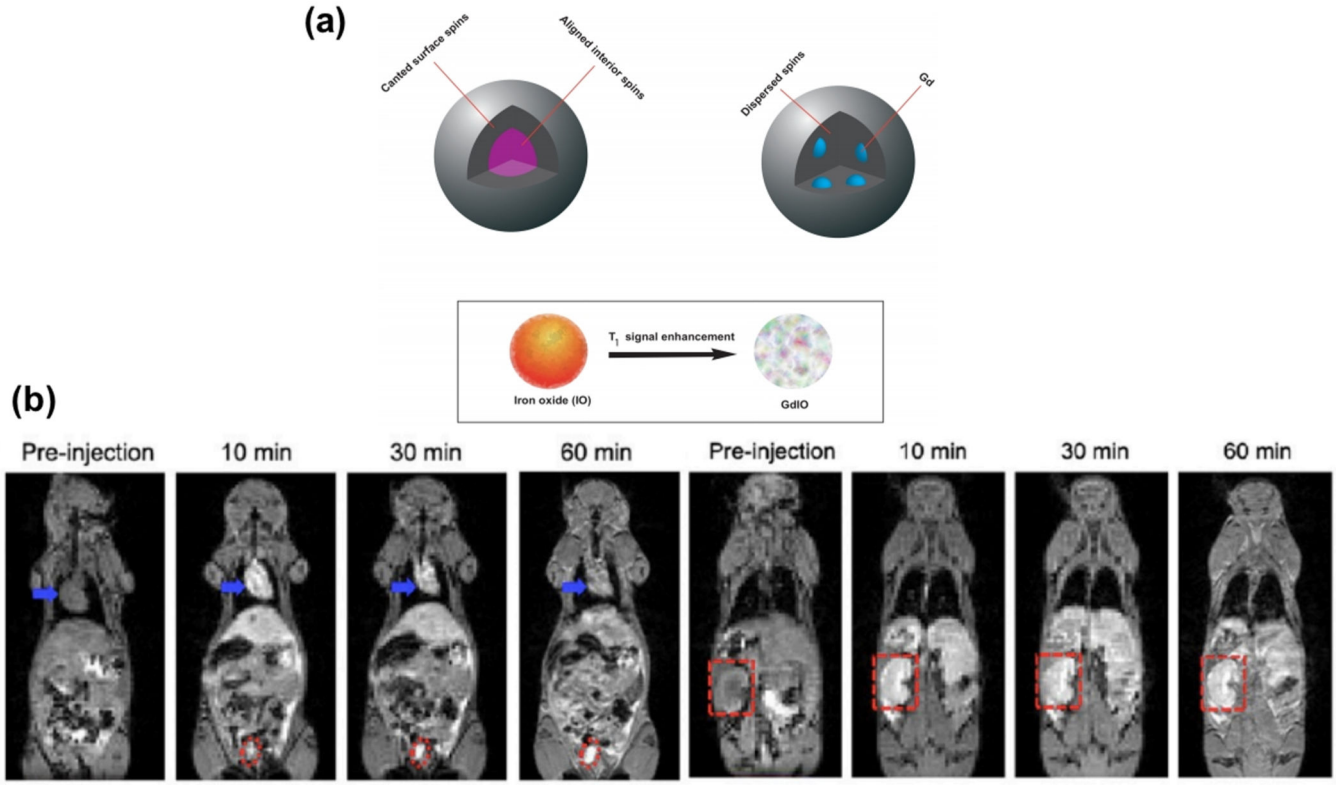

Figure 9.

(a) Schematic representation of spin canted phenomena in small-sized GdIO and IO NPs. Embedding Gd in IONPs increases the thickness of the spin canted layer and this phenomenon improves T_1 MR image contrast and brightness. Adapted with permission from Zhou *et al.* [41] Copyright (2013) American Chemical Society. (b) *In vivo* T_1-weighted MR images of mice after injection GdIO NPs with a dose of 2.0 mg GdIO NPs per kg of mice at different time points. Blue arrows, red dot, and red dashed squares correspond to heart, Bladder, and kidney, respectively. Reprinted with permission from Zhou *et al.* [41] Copyright (2013) American Chemical Society.

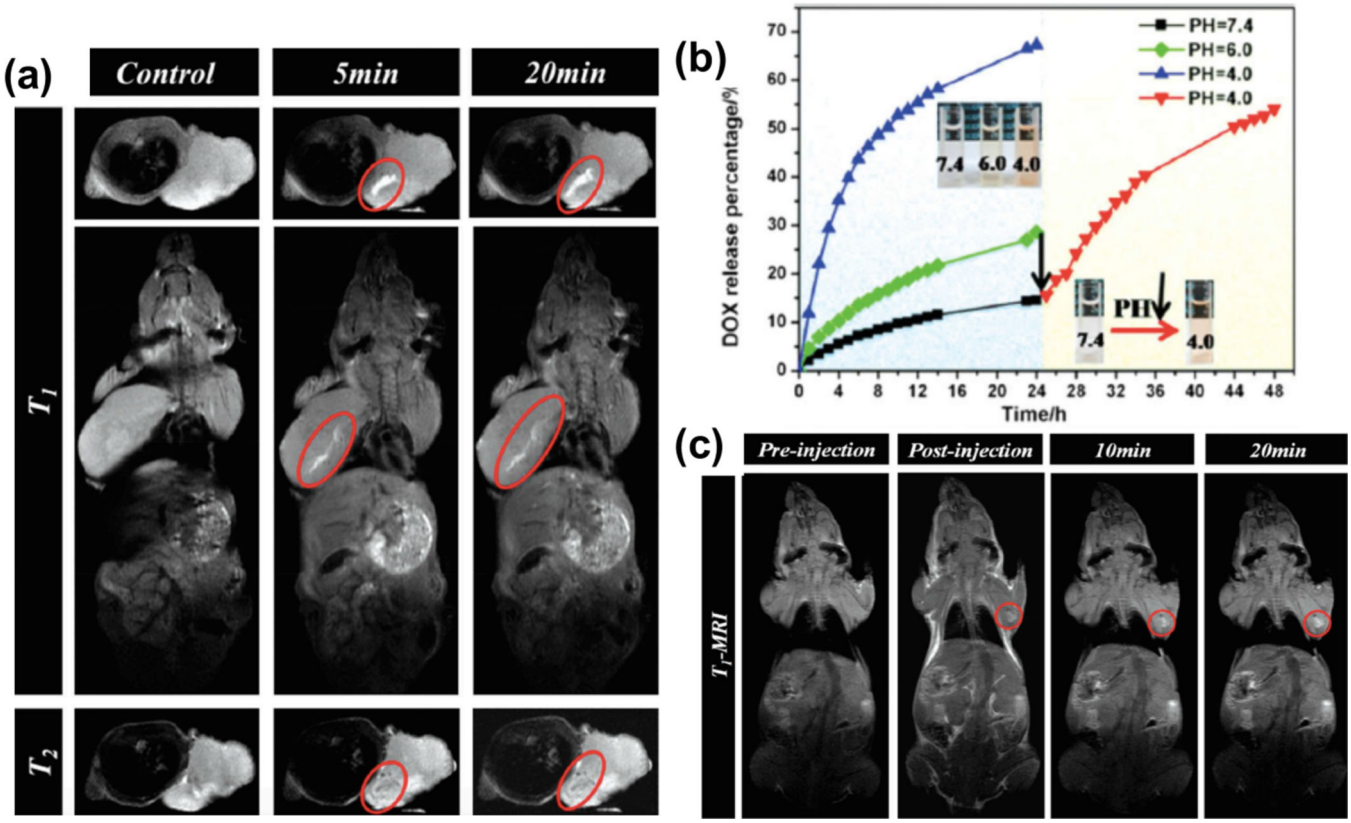

Figure 10.

(a) *In vivo* MR images from a mouse body after injection of MSNs-IONPs. (b) DOX drug release from MSNs-iron oxide pH-responsive carrier systems at different pH values. (c) *In vivo* MR images from a mouse body after injection of MSNs-DOX-IONPs. (a-c) Reprinted with permission from Wu *et al.* [204] Copyright (2014) Wiley-VCH 2014.

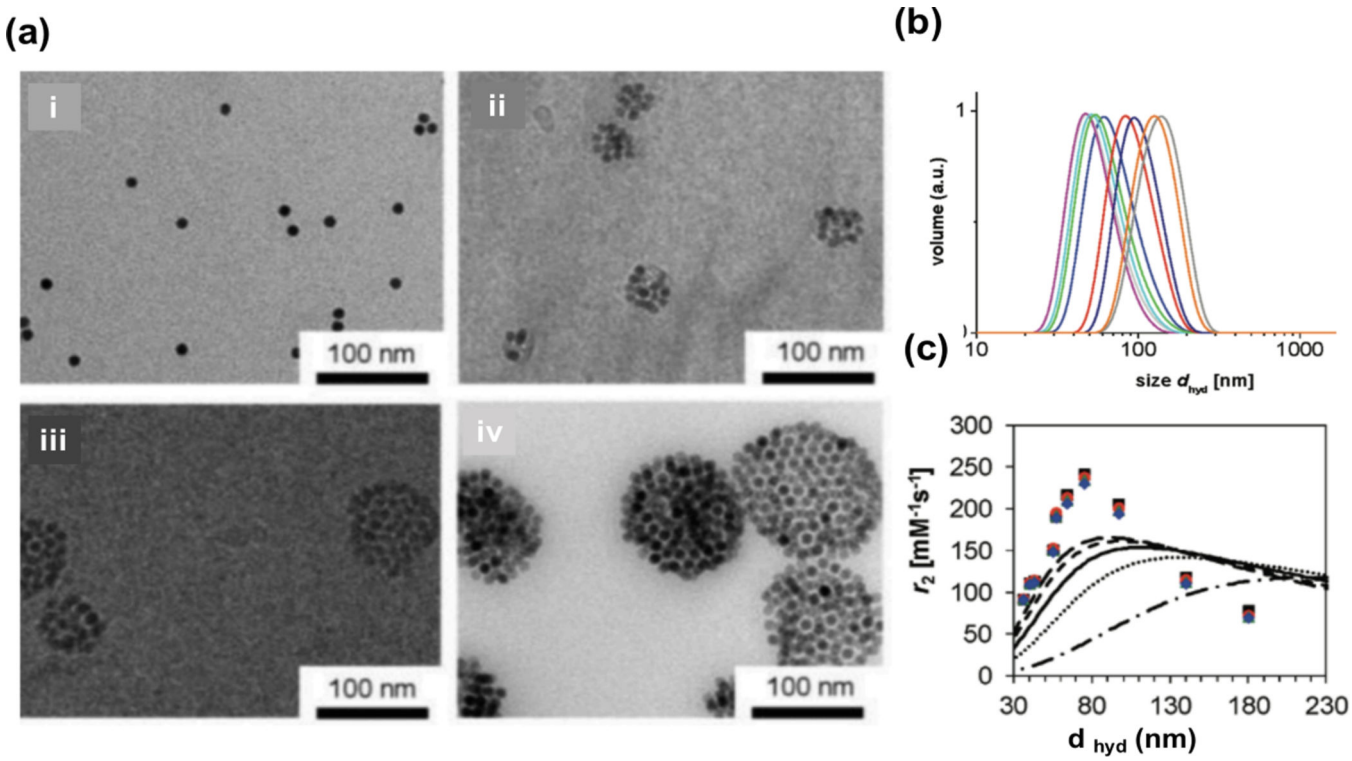

Figure 11.

(a) TEM images from single and clustered SPIONs reveal that dynamic diameter is (i) 51 nm, (ii) 70 nm, (iii) 79 nm, and (iv) 141 nm. (b) DLS volume distributions of PEI-b-PCL-b-PEG micelles with 9.8 nm superparamagnetic iron oxide (SPIO) crystals. Volume distribution of a series of different sized micelles with 9.8 nm SPION shows the average hydrodynamic of different micelles can be assumed between 51 and 141 nm. (c) The r_2 relaxivities of single and clustered IONPs versus the hydrodynamic diameters. The organic layer of the SPIO nanocrystals with a measured thickness of 0.25 nm (– –), 0.5 nm (- - -), 1 nm (——), 2 nm (. . .), and 5 nm (–·–·-). (a-c) Reprinted with permission from Pöselt *et al.* [214] Copyright (2012) American Chemical Society.

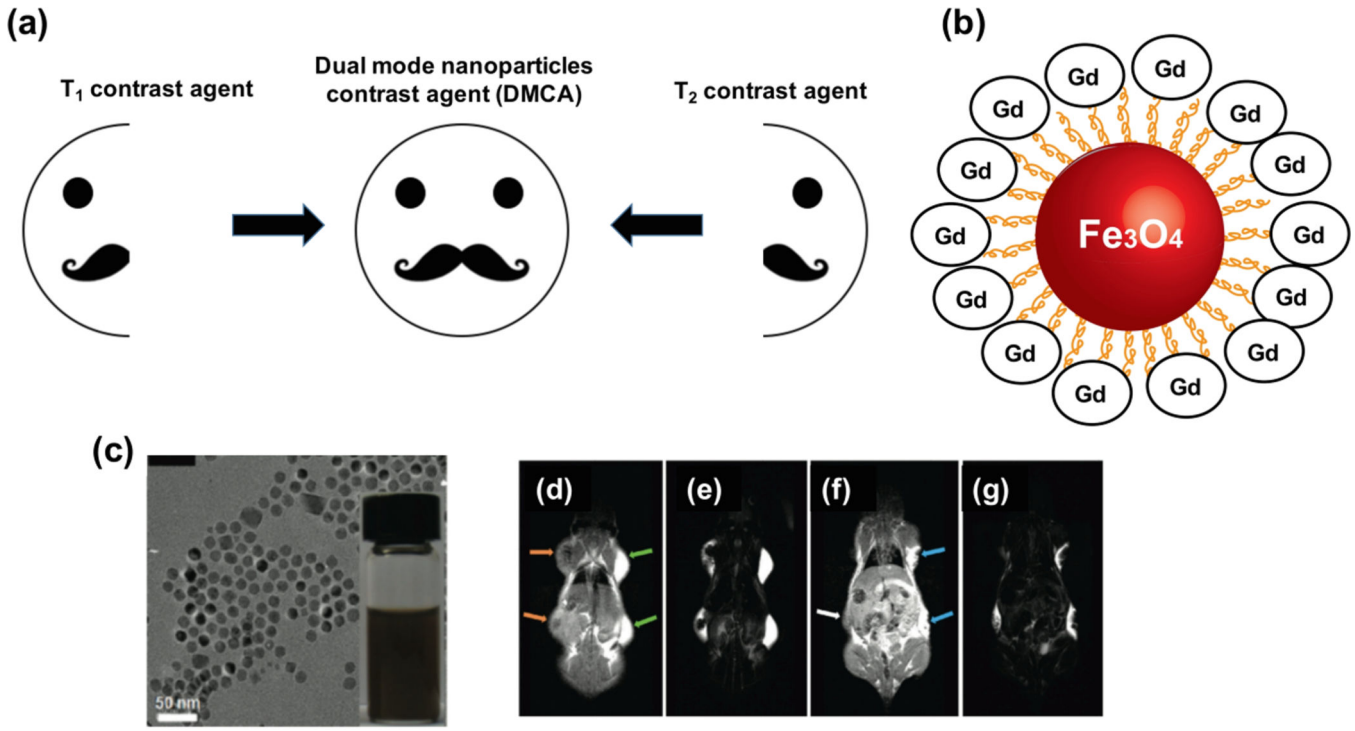

Figure 12.

(a) Schematic presentation of the ability of T_1 and T_2-weighted MR image contrast agents. (b) Schematic illustration of synthesized GMNPs. (c) A TEM image of synthesized gadolinium-labeled MNPs. (d) T_1-weighted and (e) T_2 –weighted MR images after injecting Feridex (orange arrows) and Magnevist (green arrows). (f) T_1-weighted and (g) T_2 – weighted MRI of a mouse following the injection of synthesized GMNPs (the injection site is remarked by blue arrows). (c-g) Reprinted with permission from Bae *et al.* [239]. Copyright (2010) American Chemical Society.

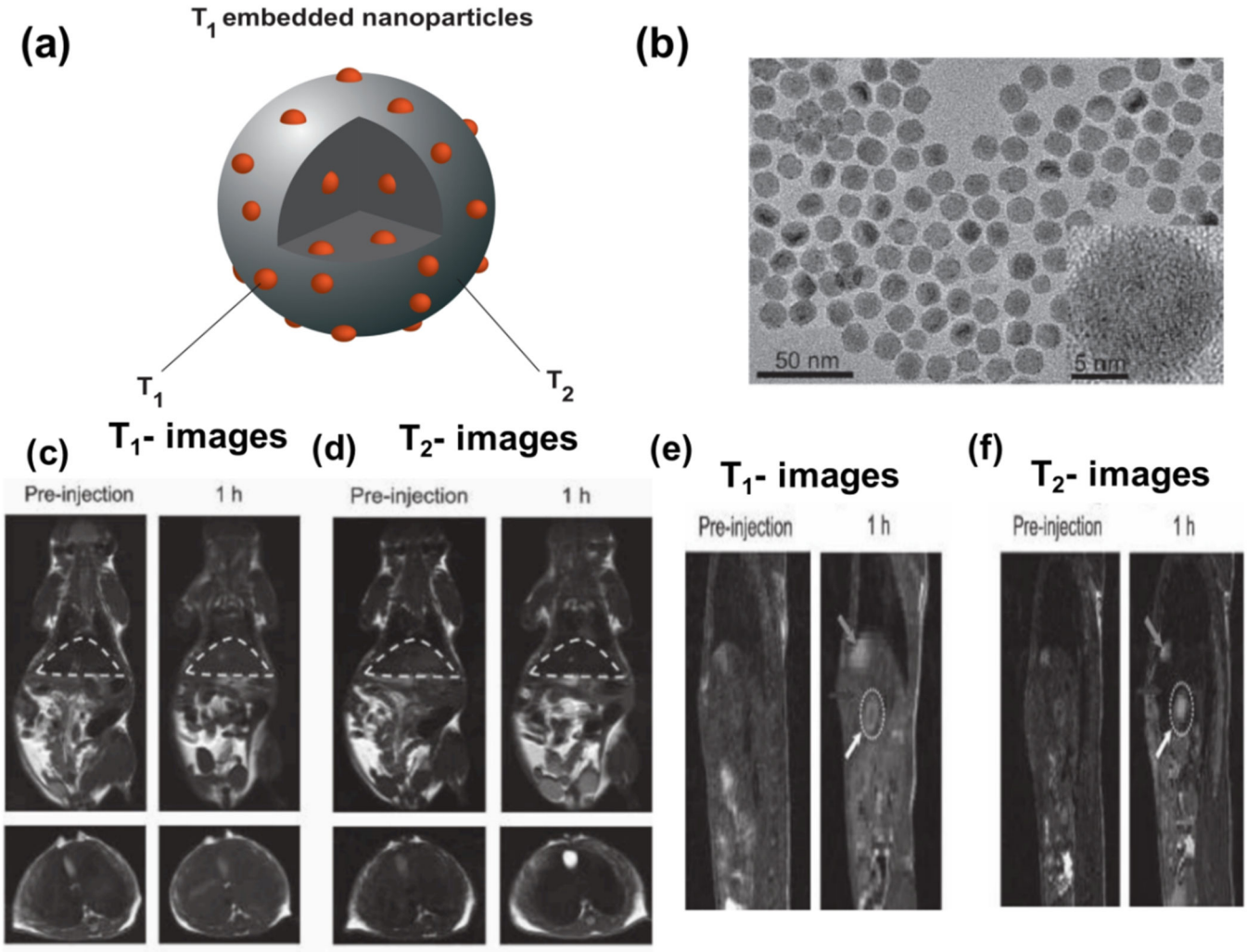

Figure 13.

(a) Schematic of embedded T_1 MRI contrast agent inside T_2 MRI contrast NP. (b) A TEM image of synthesized Gd_2O_3 (as T_1 contrast agent) inside the IONP. (c) T_1-weighted and (d) T_2-weighted in-vivo MR images before and after injection of synthesized GdIOs NPs inside a BALB/c mouse (top: coronal plane, bottom: transverse plane). (e) T_1-weighted and (f) T_2-weighted in-vivo MR images by injection of synthesized GdIOs NPs inside nude mice. Grey arrows: gallbladder, black arrows: liver, white dotted circles and white arrows: liver tumor. (a-f) Reprinted with permission from Zhou *et al.* [42] Copyright (2012) Wiley-VCH.

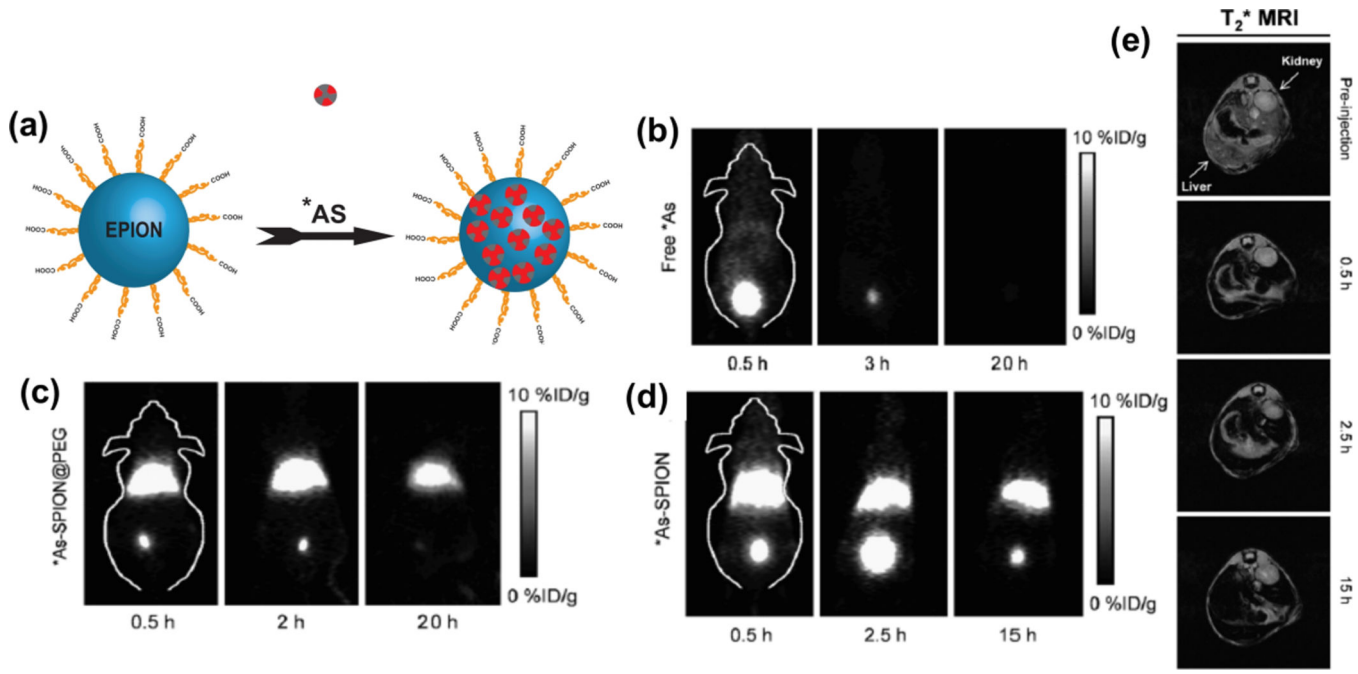

Figure 14.

(a) Schematic illustration of synthesized *As-SPIONs as dual MRI/PET contrast agents. *In vivo* PET images of BALB/c mice following injecting (b) free *As, (c) As- SPION@ PEG, and (d) *As-SPIONs. (e) *In vivo* T_2*-weighted MR images from mice before and after injection of radiolabeled As SPION. (a-e) Reprinted with permission from Chen *et al.* [247] Copyright (2013) Wiley-VCH.

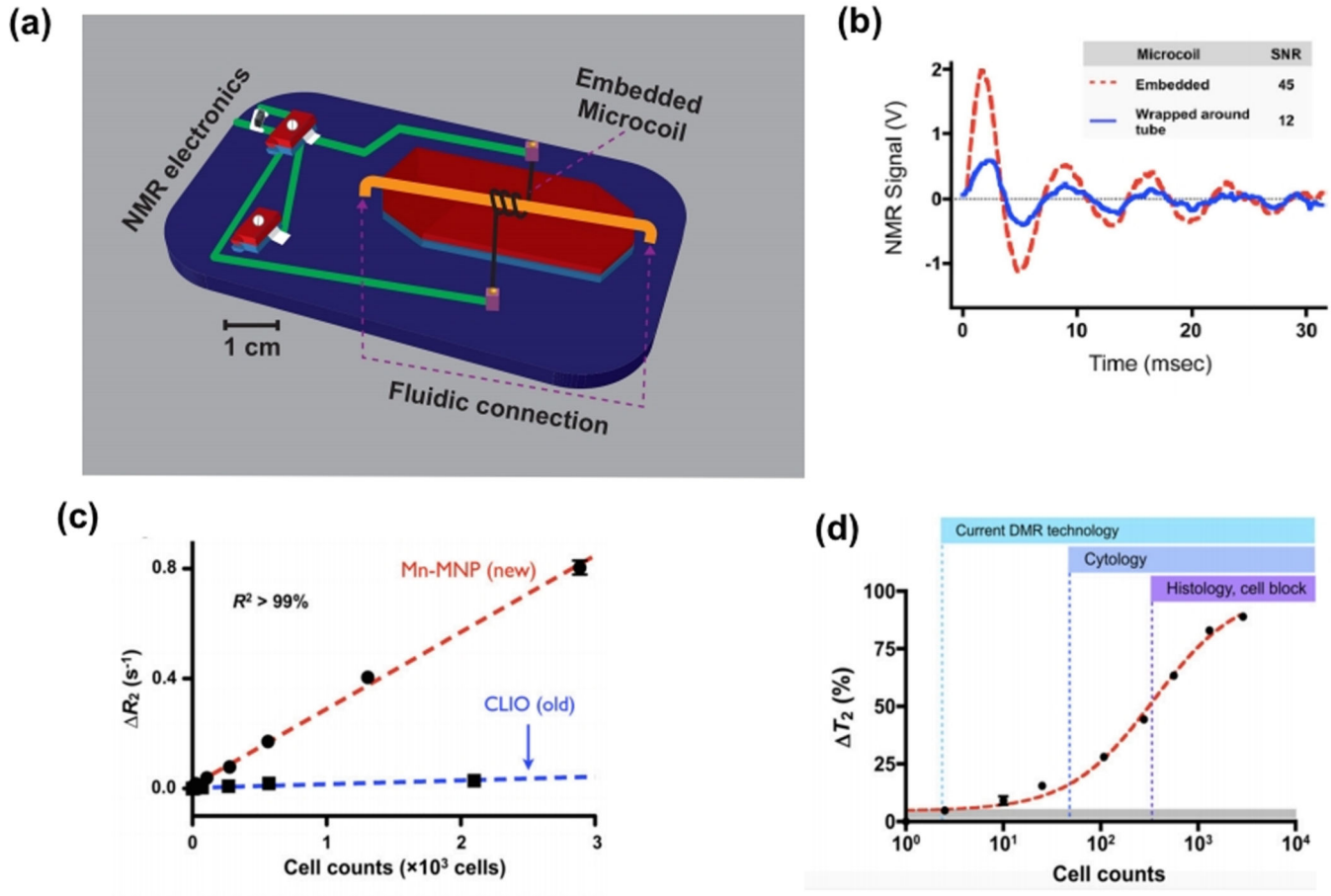

Figure 15.

(a) Schematic illustration of a DMR system with higher sensitivity developed by Lee *et al.* [11a] (b) The modification of the old planar micro-coil system by solenoidal coil embedded in a microfluidic system results in a 350% improvement in signal level. (c) Changes of $r_2 = 1/T_2$ by using BT474 cells (human breast tumor cells) labeled with CLIO NPs and developed $MnFe_2O_4$ NPs. Results show × 10 better detection sensitivity by using $MnFe_2O_4$ NPs. (d) Using $MnFe_2O_4$ NPs in DMR system enhanced sensitivity detection to a single-cell level (~2 cells). This developed DMR system has excellent properties compared to older ones such as cytology and histology. (a-d) Reprinted with permission from Lee *et al.* [11a] Copyright (2009) United States National Academy of Sciences.

Table 1:

Examples of MNPs employed in cancer therapy and diagnosis.

Nanoparticle composition	Size (nm)	Loaded drug	Application	Ref.
Composite polymeric nanoparticle composed of $MnFe_2O_4$ and poly-N isopropylacrylamide-co -poly glutamic acid	17± 2	Curcumin	pH-sensitive and thermally responsive for hyperthermia and targeted drug release	[15]
Core: Iron oxide nanoparticle Shell: polyethyleneglycol and Luteinizing Hormone–Releasing Hormone (LHRH) peptide	36.5	Doxorubicin	Chemotherapeutic drug and mild hyperthermia	[37]
Core: iron oxide Shell: chitosan	50	Temozolomide	Drug delivery to brain cancer cells	[38]
Poly (N -isopropylacrylamide-co-acrylamide)-block-poly (ɛ-caprolactone) copolymer micelles with loaded iron oxide	70	Doxorubicin	Hyperthermia (high efficiency of direct energy heating) and temporal and spatial drug release	[39]
Core: iron oxide Shell: polyvinyl alcohol (PVA)	75	Doxorubicin Paclitaxel	Drug releasing vehicle under an external magnetic field for treating breast and cervical cancer models	[40]
Gadolinium-embedded iron oxide (GdIO)	4.8	None	T_1 MRI contrast agent	[41]
Gd_2O_3 embedding in iron oxide nanoparticles	14	None	T_1-T_2 dual-mode MRI contrast agent	[42]
Core: iron oxide Shell: chitosan, PEG and PEI	40	Apurinic endonuclease 1 suppressing siRNA	Drug delivery to brain cancer cells; the siRNA decreases performance of an enzyme implicated in radiation resistance in tumors	[43]
Hybrid nanoparticle (iron oxide and gold nanoparticle)	10	None	Dual MRI and CT contrast agent	[44]
Iron oxide	35	None	T_2 MRI contrast agent	[45]
Core: iron oxide Shell: APTES	15	None	Photodynamic therapy and dual-mode fluorescence/MR imaging of epithelial cancerous cells	[46]